THE ASTRONOMICAL JOURNAL, 121:1799–1820, 2001 April

ABSORPTION SYSTEMS IN THE SPECTRA OF 66 $z \gtrsim 4$ QUASARS

CÉLINE PÉROUX
Institute of Astronomy, Madingley Road, Cambridge CB3 OHA, England, UK; celine@ast.cam.ac.uk
LISA J. STORRIE-LOMBARDI
SIRTF Science Center, California Institute of Technology, MS 100-22, Pasadena, CA 91125
RICHARD G. MCMAHON AND MIKE IRWIN
Institute of Astronomy, Madingley Road, Cambridge CB3 OHA, England, UK
AND
ISOBEL M. HOOK
Institute for Astronomy, Royal Observatory, Blackford Hill, Edinburgh EH9 3HJ, England, UK
Received 2000 November 27; accepted 2001 January 9

ABSTRACT

We present high signal-to-noise, ~ 5 Å resolution (FWHM) spectra of 66 $z \gtrsim 4$ bright quasars obtained with the 4 m Cerro Tololo Inter-American Observatory and 4.2 m William Hershel telescopes. The primary goal of these observations was to undertake a new survey for intervening absorption systems detected in the spectra of background quasars. We look for both Lyman-limit systems (column densities $N_{\rm H\,I} \geq 1.6 \times 10^{17}$ atoms cm^{-2}) and damped Lyα systems (column densities $N_{\rm H\,I} \geq 2 \times 10^{20}$ atoms cm^{-2}). This work resulted in the discovery of 49 Lyman-limit systems, 15 of which are within 3000 km s^{-1} of the quasar emission and thus might be associated with the quasar itself, 26 new damped Lyα absorption candidates, 15 of which have $z > 3.5$, and numerous metal absorption systems. In addition, 10 of the quasars presented here exhibit intrinsic broad absorption lines.

Key words: galaxies: evolution — galaxies: high-redshift — line: identification — quasars: absorption lines — quasars: general — surveys

On-line material: machine-readable table

1. INTRODUCTION

Because they are extremely luminous, quasars are among the youngest objects observed in the universe and have now been detected out to redshifts of $z \sim 5.8$ (Fan et al. 2000). Observing quasars at such high redshifts gives us direct indications of the ionization state of the early universe. Indeed, the lack of an observed Gunn-Peterson effect (Gunn & Peterson 1965) indicates that the universe is already ionized at these early epochs.

In addition to being important observations in their own right, spectroscopic studies of quasars allow the detection of much fainter systems, observed in absorption in the quasar spectra. There are two main classes of quasar absorption lines: the metal systems, such as C IV or Mg II, and the more numerous hydrogen lines. The latter are subdivided into three different groups according to their neutral hydrogen column densities. The Lyα forest absorbers have column densities 10^{12}–1.6×10^{17} atoms cm^{-2}. The Lyman-limit systems (LLSs) have $N_{\rm H\,I} \geq 1.6 \times 10^{17}$ atoms cm^{-2} and the damped Lyα systems (DLAs) are a subset of the LLSs with $N_{\rm H\,I} \geq 2 \times 10^{20}$ atoms cm^{-2}. They thus probe media with different column densities spanning the range from voids through to halos and disks of both dwarf and normal (proto) galaxies. The morphology of DLAs in particular is still open to debate. The hypotheses put forward range through large disk systems (Prochaska & Wolfe 1998), low surface brightness galaxies (Jimenez, Bowen, & Matteucci 1999) and dwarf galaxies (Matteucci, Molaro, & Vladilo 1997). Although the exact nature of the quasar absorbers is not known, they form a sample of systems unbiased as regards luminosity, specific morphology, metallicity, or emission line strength, thus enabling studies of metallicity and H I evolution over a large redshift range.

The primary goal of our spectroscopic campaign is to obtain a statistically significant number of high-redshift absorbers to answer the questions raised by the apparent deficit of high column density systems at such redshifts (Storrie-Lombardi et al. 1996c; Storrie-Lombardi & Wolfe 2000). In particular we aim to study in more detail the evolution with redshift of the column density distribution, number density, and comoving mass density of high column density H I absorption systems. The latter has been quite controversial in the last few years. Lanzetta, Wolfe, & Turnshek (1995) found that $\Omega_{\rm DLA}$ at $z \sim 3.5$ is twice the value at $z \sim 2$, implying a larger star formation rate than indicated by metallicity studies. This created the so-called "cosmic G-dwarf problem." Storrie-Lombardi, McMahon, & Irwin (1996b) used new data to show that $\Omega_{\rm DLA}$ decreases at high redshift thus solving the "cosmic G-dwarf problem." The work of Storrie-Lombardi & Wolfe (2000) confirmed such results by using a compilation of data gathered from the literature together with new spectroscopic observations. The aim of our new survey for quasar absorbers is to better understand the high-redshift end of the mass density of neutral hydrogen by significantly improving the statistics at $z \gtrsim 3.5$. At low redshift, recent studies by Rao & Turnshek (2000) show that $\Omega_{\rm DLA}$ might be higher than first expected. Their analysis is based on *HST* observations of quasars with known Mg II systems (Mg II always being associated with DLA systems, the reverse not being true). Nevertheless it should be emphasized, as the authors themselves pointed out, that the analysis is based on a relatively small number of systems. At all redshifts such measurements can be used to constrain the most recent semianalytical models of galaxy formation (Kauffmann & Haehnelt 2000 and Somerville, Primack, & Faber 2000, which build on models originally presented by Kauffmann, White, & Guiderdoni 1993 and Cole et al. 1994). Several fundamental questions remain including locating the epoch of DLAs assembly, clarifying the relationship between Lyman limit systems and damped absorbers, measuring the total amount of neutral hydrogen contained in quasar absorbers, and studying how this varies with redshift. We will discuss the impact of our new survey on these issues in more detail in future papers currently in preparation (Peroux et al. 2001).

Any survey for quasar absorbers begins with a search for bright quasars and so constitutes an ambitious observational program. We observed 66 $z \gtrsim 4$ quasars discovered by various groups (Storrie-Lombardi et al. 2001; Fan et al. 1999; Warren, Hewett, & Osmer 1991; Kennefick et al. 1995a; Storrie-Lombardi et al. 1996c; Zickgraf et al. 1997; Kennefick, Djorgovski, & De Carvalho 1995b; Henry et al. 1994; Hook et al. 2001, in preparation; Hall et al. 1996) almost all of which have not been previously studied at such resolution (≈ 5 Å) and signal-to-noise (ranging from 10 to 30). We obtained optical spectra at the 4.2 m William Herschel Telescope for the northern quasars and at the 4 m Cerro Tololo Inter-American Observatory for the southern objects. More information about $z \gtrsim 4$ quasars is available at the following URL: http://www.ast.cam.ac.uk/~quasars.

This paper is organized as follows. In § 2 we provide the details of the setup for each observational run and in § 3 describe the data reduction and present the quasar spectra. Accurate quasar redshift and magnitude measurements are given in § 4. The surveys for Lyman-limit systems and damped Lyα absorbers are presented in §§ 5 and 6, respectively. Provisional interpretation of metal absorption features are summarized in § 7. Notes on individual objects are provided in § 8, and conclusions are presented in § 9.

2. OBSERVATIONS

All the new observations were carried out during two observing runs at the 4.2 m William Herschel telescope (WHT) of the Isaac Newton Group of telescopes in the Canary Islands and two observing runs at the Blanco 4 m telescope at the Cerro Tololo Inter-American Observatory (CTIO) in Chile. High signal-to-noise optical spectrophotometry was obtained covering approximately 3500–9000 Å, the exact range depending on which instrument was used for the observations. A journal of the observations is presented in Table 1.

Thirty-one (including a $z = 1.90$ quasar PSS J0052+2405) quasars were observed at the WHT during 1998 September 22–24 and 1999 March 18–19. The integration times were typically 1800–3600 s. We used the ISIS double-spectrograph, which consists of two independent arms fed via a dichroic allowing for blue and red observations to be carried out simultaneously. Gratings with 158 lines mm^{-1} and a dichroic to split the light at $\sim$5700 Å were used. This gives a dispersion of 2.89 Å pixel^{-1} in the red arm and 1.62 Å pixel^{-1} in the blue. The gratings were arranged so that the blue part of the spectrum was centered on 4500 Å, while the red was centered on 7000 Å. On the blue arm a thinned coated English Electric Valve (EEV) 2148 × 4200 CCD with 13.5 μm pixels was used as detector. On the red arm a thinned coated Tektronix 1124 × 1124 CCD with 24 μm pixels was used. All the narrow-slit observations were taken with a slit width of 1''.2–1''.5, while the wide-slit observations were carried out with a slit width of 5''–7''. Blind-offsetting from bright $\sim$15–17 mag stellar fiducials was used to position the quasars in the slit partly to save acquisition time and partly because the majority of the quasars were not visible using the blue sensitive TV acquisition system. Readout time was reduced by windowing the CCDs in the spatial direction.

Thirty-five quasars were observed at CTIO during 1998 October 14–16, and 1999 October 9–12. The typical exposure time was 3600 s for the brighter objects ($R \sim$ 18–19 mag) but substantially longer times were used for the fainter Sloan Digital Sky Survey quasars. We used the R-C spectrograph with the 316 lines mm^{-1} grating, centered at 6050 Å and covering the range 3000–9100 Å. This setup resulted in a dispersion of 1.98 Å pixel^{-1}. The detector used was a Loral 3072 × 1024 CCD detector. The narrow and wide slit observations were taken with 1''–1''.5 and 5'' widths, respectively. Because of the substantial wavelength coverage available with this setup we used a WG345 blocking filter (with 50% transmission at 3450 Å) to minimize the second-order contamination from the standard stars above 7000 Å. The contamination is negligible for the quasars as most have no flux below 4500 Å but affects the standard stars that have substantial flux at 3500 Å. Appropriate mea-

TABLE 1
Journal of Observations

Quasar Name	Observed Telescope	Observed Date	Exposure Time B/R^a(s)	Wide Slit	Reference
PSS J0003+2730	WHT	1998 Sep 22	3600/3600	Yes	1
BR J0006−6208.........	CTIO	1998 Oct 14	3600	Yes	3
BR J0030−5129.........	CTIO	1998 Oct 15	3600	Yes	3
PSS J0034+1639	WHT	1998 Sep 22	3600/3600	Yes	1
SDSS J0035+0040......	CTIO	1999 Oct 10	8100	Yes	4
PSS J0052+2405	WHT	1998 Sep 23	3600/3600	Yes	2
Q J0054−2742	CTIO	1999 Oct 12	2700	Yes	5
PSS J0106+2601	WHT	1998 Sep 24	3600/3600	Yes	1
PSS J0131+0633	CTIO	1999 Oct 12	3600	No	2
PSS J0133+0400	CTIO	1999 Oct 12	3600	No	2
PSS J0134+3307	WHT	1998 Sep 22	3600/3600	Yes	1
PSS J0137+2837	WHT	1998 Sep 24	5200/3600	Yes	1
PSS J0152+0735	WHT	1998 Sep 24	3600/3600	Yes	1

TABLE 1—*Continued*

Quasar Name	Observed: Telescope	Observed: Date	Exposure Time B/R^a(s)	Wide Slit	Reference
PSS J0207+0940	CTIO	1999 Oct 12	3600	No	2
PSS J0209+0517	CTIO	1999 Oct 12	2400	No	2
SDSS J0211−0009	CTIO	1999 Oct 10	8100	No	4
BR J0234−1806	CTIO	1999 Oct 09	5400	Yes	3
PSS J0248+1802	WHT	1998 Sep 22	3600/3600	Yes	6
BR J0301−5537	CTIO	1998 Oct 16	3600	Yes	3
BR J0307−4945	CTIO	1998 Oct 14	5400	Yes	3
SDSS J0310−0014	CTIO	1999 Oct 9	9900	No	4
BR J0311−1722	CTIO	1999 Oct 11	3600	Yes	3
PSS J0320+0208	CTIO	1999 Oct 12	3600	No	2
BR J0324−2918	CTIO	1999 Oct 11	3600	Yes	3
BR J0334−1612	WHT	1998 Sep 23	2740/1650	No	3
SDSS J0338+0021	Keck	1999 Feb 17	3000/3600	No	4
BR J0355−3811	CTIO	1998 Oct 15	3600	Yes	3
BR J0403−1703	WHT	1999 Sep 19	1800/1800	No	7
BR J0415−4357	CTIO	1998 Oct 16	5400	Yes	3
BR J0419−5716	CTIO	1998 Oct 14	3600	Yes	3
BR J0426−2202	CTIO	1999 Oct 11	3000	Yes	3
PMN J0525−3343	CTIO	1998 Oct 15	3600	Yes	3
BR J0529−3526	CTIO	1998 Oct 14	5400	Yes	3
BR J0529−3552	CTIO	1998 Oct 15	3600	Yes	3
BR J0714−6455	CTIO	1998 Oct 15	3600	Yes	3
PSS J0747+4434	WHT	1998 Sep 22	1800/1800	No	1
RX J1028−0844	WHT	1999 Mar 19	2700/2700	Yes	8
PSS J1048+4407	WHT	1999 Mar 19	2700/2700	Yes	9
PSS J1057+4555	WHT	1999 Mar 19	1800/1800	Yes	9
PSS J1159+1337	WHT	1999 Mar 18	2700/2700	Yes	1
PSS J1253−0228	WHT	1999 Mar 18	2700/1800	Yes	2
BR J1310−1740	WHT	1999 Mar 19	2700/2700	Yes	3
BR J1330−2522	WHT	1999 Mar 19	2700/2700	Yes	3
FIRST J1410+3409......	WHT	1999 Sep 19	2700/2700	Yes	1
PSS J1438+2538	WHT	1999 Mar 18	2700/2700	Yes	9
PSS J1456+2007	WHT	1999 Mar 18	2700/2700	Yes	1
BR J1603+0721	WHT	1999 Mar 19	2700/2700	Yes	3
PSS J1618+4125	WHT	1999 Mar 19	2700/2700	Yes	1
PSS J1633+1411	WHT	1999 Mar 19	1800/1800	Yes	2
PSS J1646+5514	WHT	1998 Sep 23	3600/3600	Yes	1
PSS J1721+3256	WHT	1998 Sep 24	1800/3600	Yes	1
RX J1759+6638	WHT	1999/1998 Mar 19/Sep 23	6300/6300	Yes	10
PSS J1802+5616	WHT	1999 Sep 14	1800	No	2
BR J2017−4019	CTIO	1998 Oct 14	3600	No	3
PSS J2122−0014	WHT	1998 Sep 22	3600/3600	No	1
BR J2131−4429	CTIO	1998 Oct 16	1800	No	3
PMN J2134−0419	CTIO	1999 Oct 12	5400	Yes	11
PSS J2154+0335	WHT	1999 Sep 14	1800	No	2
PSS J2155+1358	CTIO	1999 Oct 10	3600	Yes	2
BR J2216−6714	CTIO	1999 Oct 09	3600	Yes	3
PSS J2241+1352	CTIO	1999 Oct 11	3600	Yes	2
DMS B2247−0209.......	WHT	1998 Sep 24	5400/3600	Yes	12
PSS J2315+0921	CTIO	1999 Oct 11	3600	Yes	2
BR J2317−4345	CTIO	1998 Oct 14	3600	Yes	3
BR J2328−4513	CTIO	1998 Oct 15	3600	Yes	3
PSS J2344+0342	CTIO	1999 Oct 11	3600	Yes	2
BR J2349−3712	CTIO	1999 Oct 09	3600	Yes	3

Notes.—The quasar prefixes indication the following origin: (BR) APM survey objects selected by B_J-R color excess; (PSS) Second Palomar Sky Survey; (PMN) Parkes-MIT-NRAO radio-selected objects; (RX) X-ray selected; (SDSS) Sloan Digital Sky Survey; (DMS) Deep Multicolor Survey.

[a] For the quasars observed at the WHT the B/R designations give the exposure times through the blue and red arms of the ISIS spectrograph.

References.—(1) Stern et al. 2000; (2) G. Djorgovski's web site at http://www.astro.caltech.edu/~george/z4.qsos; (3) Storrie-Lombardi et al. 2001; (4) Fan et al. 1999; (5) Warren et al. 1991; (6) Kennefick et al. 1995a; (7) Storrie-Lombardi et al. 1996c; (8) Zickgraf et al. 1997; (9) Kennefick et al. 1995b; (10) Henry et al. 1994; (11) Hook et al. 2001, in preparation; (12) Hall et al. 1996.

sures, as discussed in the data reduction section, have been taken so that this setup does not modify the flux calibration at the red end of the spectra. Using two instrumental setups in order to completely remove the second-order contamination problem would have resulted in a 60%–80% increase in the required observing time.

The observations of SDSS J0338+0022 were taken at the Keck Observatory with the Low Resolution Imaging Spectrometer (LRIS). The observational details are given in Songaila et al. (1999).

3. DATA REDUCTION

The data reduction was undertaken using the IRAF[1] software package. Because the bias frames for each nights were so similar, a master "zero" frame for each run was created using the IMCOMBINE routine. The data were overscan corrected, zero corrected, and trimmed using CCDPROC. Similarly, a single flat-field frame was produced by taking the median of the Tungsten flats. The overall background variation across this frame was removed to produce an image to correct for the pixel-to-pixel sensitivity variation of the data. The task APALL was used to extract one-dimensional multispectra from the two-dimensional frames. The routine estimates the sky level by model fitting over specified regions on either side of the spectrum.

The WHT data were wavelength calibrated using CuAr and CuNe arcs and monitored using night sky lines. Arcs were taken at each object position for wavelength calibrating the CTIO data. We used solely the sky lines to wavelength calibrate the Keck data. The spectra were flux calibrated using observations taken of spectrophotometric standards. B stars free of strong features in the red were observed in order to remove the effects of atmospheric absorption in the red-arm WHT spectra and the CTIO spectra (e.g., O_2 A band at 7600 Å). The atmospheric absorption features seen in the B-star spectrum were isolated by interpolating between values on either side of the feature. The original B-star spectrum was then divided by this atmospheric-free spectrum to create an atmospheric correction spectrum. Finally, the object spectra were divided by the scaled correction spectrum. In the case of ISIS data the red and blue ends of the spectra were then joined using SCOMBINE. In all cases if a wide-slit observation was made (see Table 1), it was used to correct the absolute flux levels for slit losses.

As mentioned in § 2, the quasar spectra observed using the R-C spectrograph at CTIO suffered a gradual flux decrement in the red end calibration due to the inclusion of the second-order flux from the standard stars. In order to correct for this effect, spectra of standard stars were taken with two different blocking filters (3450 and 5000 Å). The effect of the filter at wavelengths above 8000 Å could thus be determined and a correction applied accordingly to the quasar spectra. In addition a quasar previously observed with the ISIS double-spectrograph on WHT was reobserved at CTIO and corrected as explained above. Comparing the two spectra reveals no significant difference and provides a successful double check on the method. In any case the flux calibration of the red end of the spectra is relatively unimportant for the work undertaken here, namely the search of quasar absorbers blueward of the Lyα emission.

The resulting spectra have a signal-to-noise ratio ranging from $\approx$10–30 at 7000 Å. They are shown in Figure 1 with arbitrary flux scales. Ten of the quasars presented here exhibit intrinsic broad absorption lines (BAL). The feature in all of the CTIO spectra at 8900 Å is due to bad columns. In the 1999 run, the objects were moved along the slit between exposures so the effects of the bad columns were spread over a slightly wider region of the spectrum.

4. REDSHIFT AND MAGNITUDE MEASUREMENTS

In order to measure the redshifts, Gaussians were fitted, if possible, to N V (rest wavelength 1240.13 Å), O I (1304.46 Å), Si IV + O IV] (1400.0 Å) and C IV (1549.1 Å) emission lines. The redshift for each line was determined from the central wavelength ($z = \lambda_{\rm observed}/\lambda_{\rm emitted} - 1$). Ly$\alpha$ (rest wavelength 1215.67 Å) is almost 50% absorbed by the Lyα forest, so that the blue edge of the emission line has been used for redshift determination whenever possible. Some lines were impossible to fit and made the redshift determination difficult, especially in the case of the BALs. The redshift of each emission line, their average and the 1 σ error are shown in Table 2. This error is representative of the error in the fit, in wavelength calibration (estimated to be around 0.1 Å) and in the fact that the various species are coming from different physical regions of the quasar. In practice, this latter effect is probably the dominant source of differences in the emission line redshifts.

To provide an internal check on our redshift determinations we produced a median composite quasar spectrum (Francis et al. 1991). Each non-BAL spectrum with enough wavelength coverage was corrected to the rest-frame and scaled such that the median of the flux in a region free from emission lines (1420–1470 Å) is unity. The spectra were then rebinned into fixed 0.5 Å bins (i.e., similar to the resolution in the observed frame) and the median of the flux in each bin was calculated to produce the spectrum in Figure 2. Measuring the wavelength of the emission lines of the median composite spectrum provides an estimate of any systematic bias in the redshift measurements which in our case proves to be about $z = 0.001$ (see last row of Table 2) and allows any shift in quasar redshifts to be checked by cross-correlation.

Table 3 summarizes the photometric and spectroscopic magnitudes for each object. The photometric magnitudes were measured from the UKST and POSS1 plates scanned using the APM facility. The spectroscopic magnitudes are derived from the spectra themselves using the IRAF task CALCPHOT and the "R59" (R) or "R63" (OR) filter curves for the quasars magnitudes from the UKST survey and the "e" filter curve for quasar magnitudes from POSS1 survey. These transmission curves are shown on Figure 3 overplotted on the $z = 4.172$ BR J0529−3552 quasar spectrum. The error on the spectroscopic measurements is estimated to be ± 0.1 mag, and the error on the APM R magnitude is ± 0.25 mag.

5. LYMAN-LIMIT SYSTEMS

5.1. *Background*

Lyman-limit systems (LLSs) are absorption systems with hydrogen column densities $N_{\rm H\,I} \geq 1.6 \times 10^{17}$ atoms cm^{-2}.

[1] IRAF is distributed by the National Optical Astronomy Observatories, which are operated by the Association of Universities for Research in Astronomy, Inc., under cooperative agreement with the National Science Foundation.

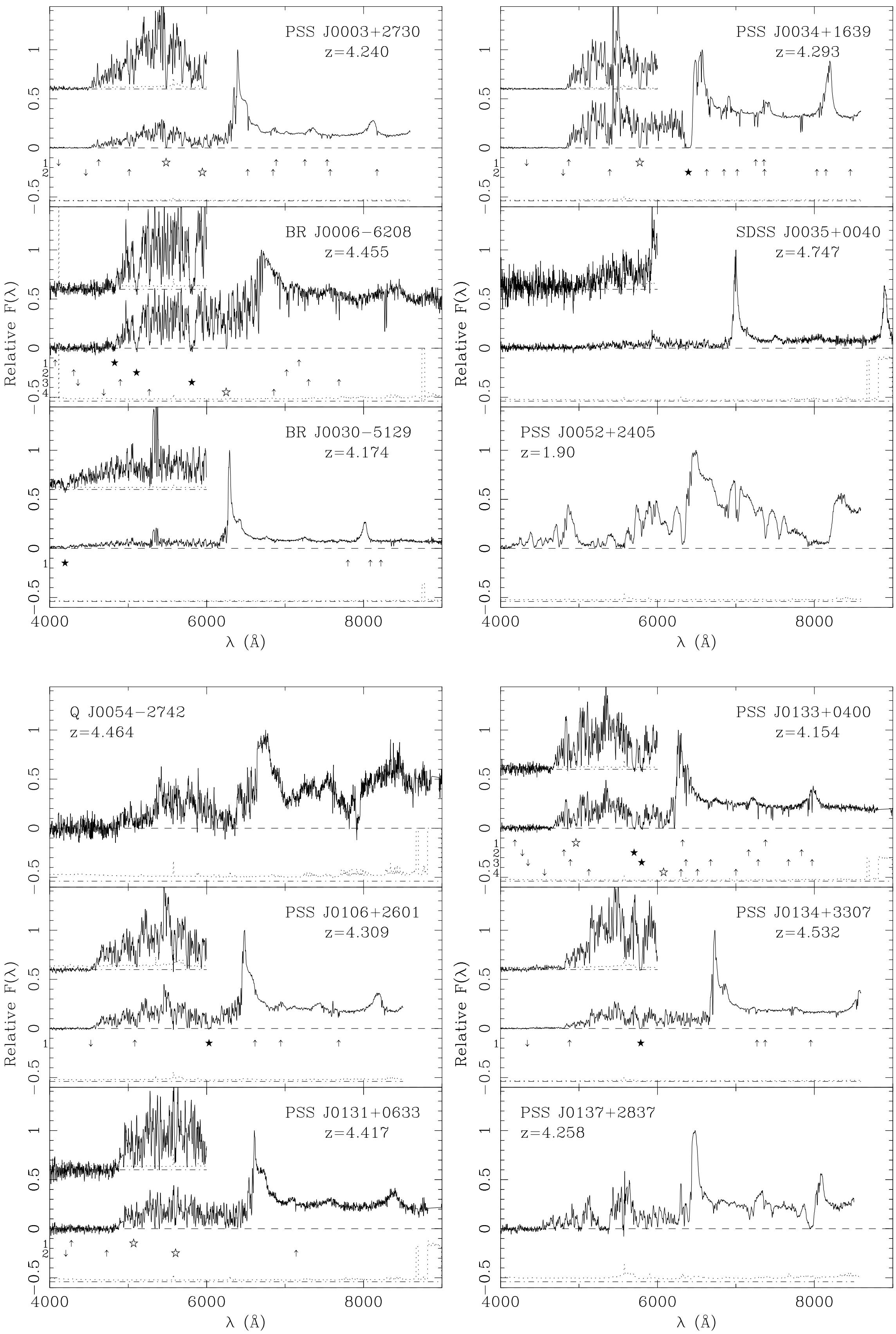

FIG. 1.—Spectra of all the observed quasars. The error arrays are plotted as dotted lines, offset below the spectra for clarity. In the upper left-hand corner, the blue region of the spectra are magnified to make the Lyman-limit systems and damped Lyα candidate absorbers easier to see. Damped Lyα candidate absorbers are marked below there positions as solid stars if they have estimated column densities $N_{\mathrm{H\,I}} \geq 2 \times 10^{20}$ atoms cm^{-2}, and as open stars if they have estimated column densities lower than this threshold, but greater than 5×10^{19} atoms cm^{-2}. To the right of the stars marking the DLA are the detected metal lines that are associated with this absorber. To the left of the stars are an upward arrow marking the position of Lyβ at the DLA redshift and a downward arrow marking the wavelength of the Lyman-limit that would be associated with this DLA.

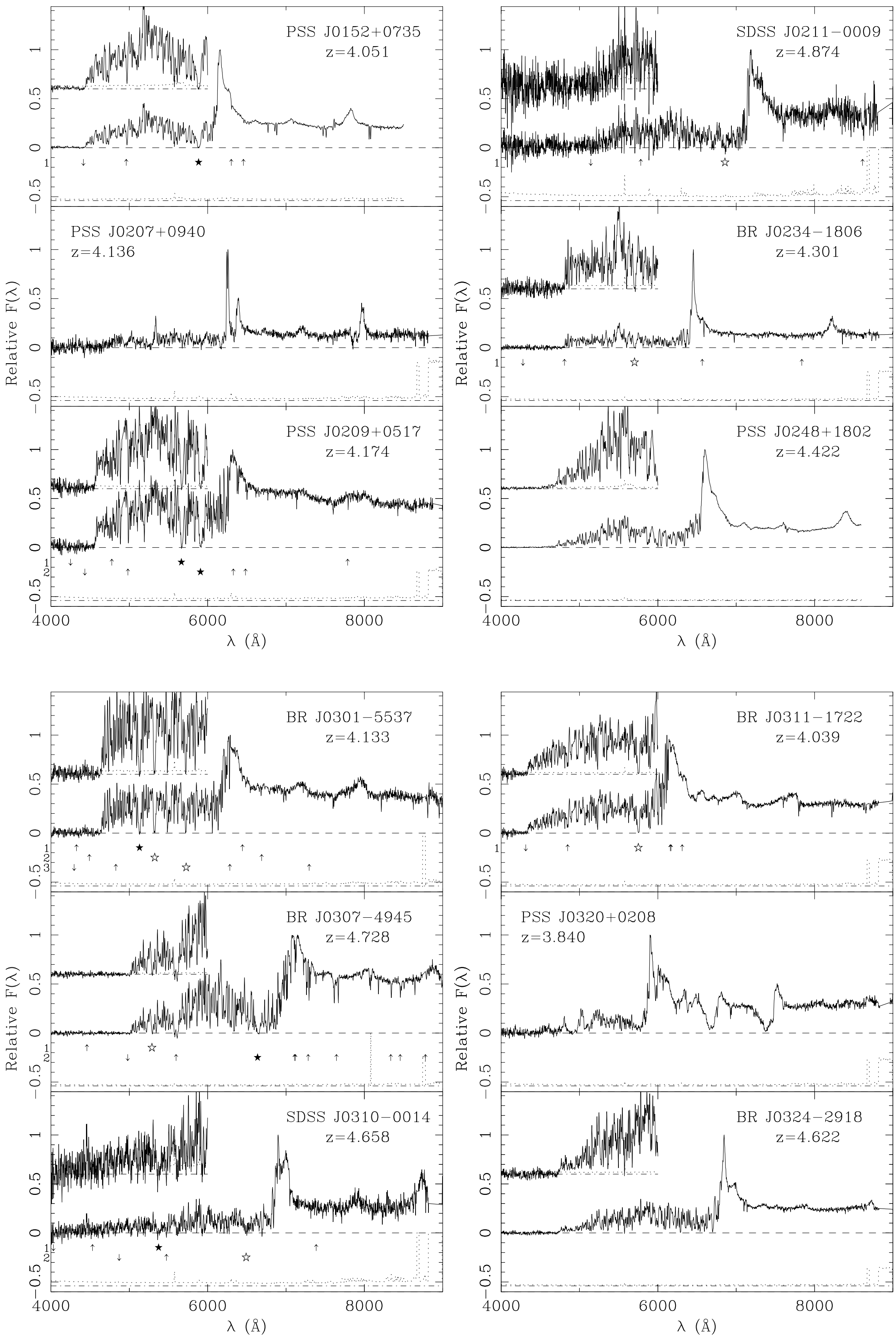

FIG. 1.—*Continued*

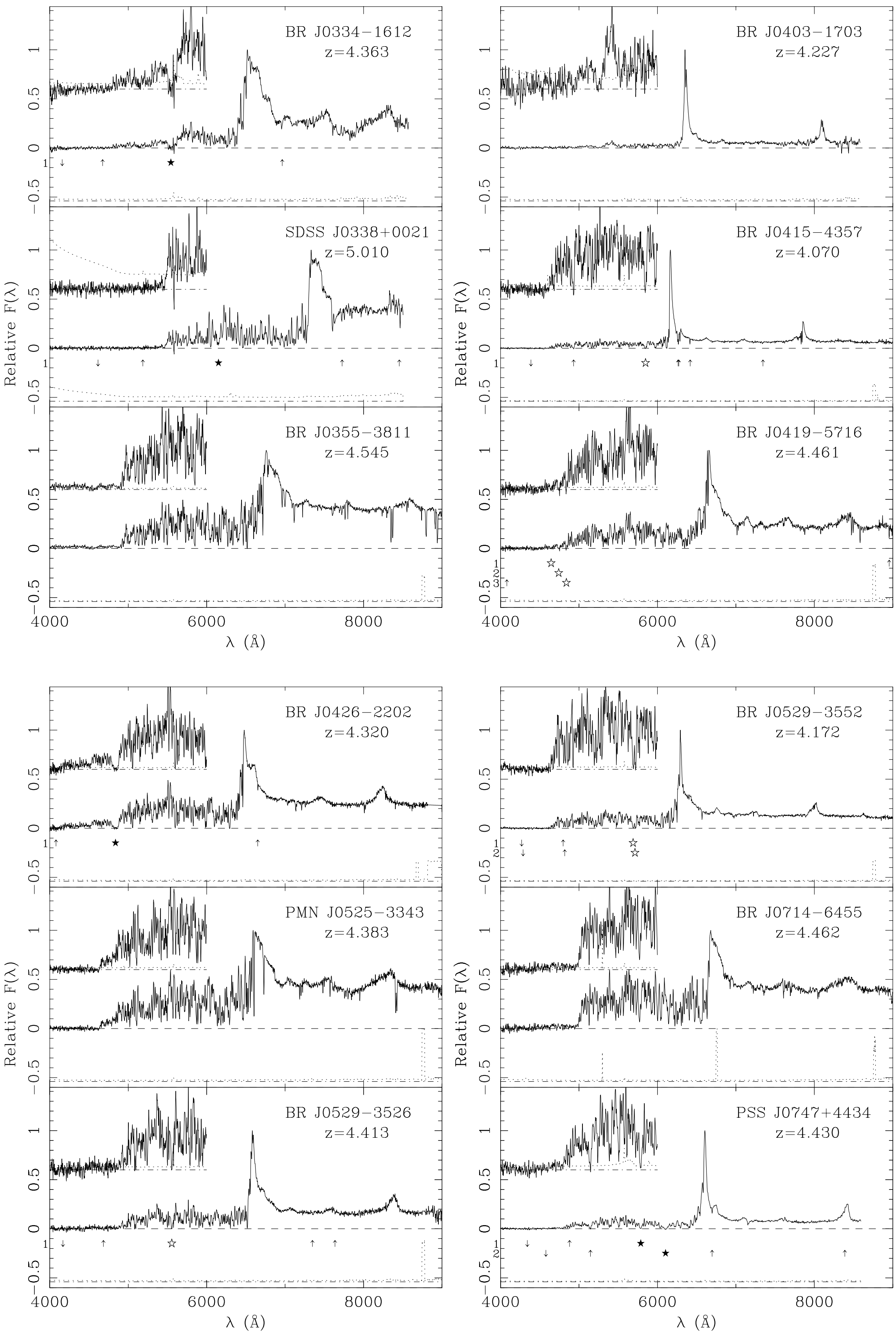

FIG. 1.—*Continued*

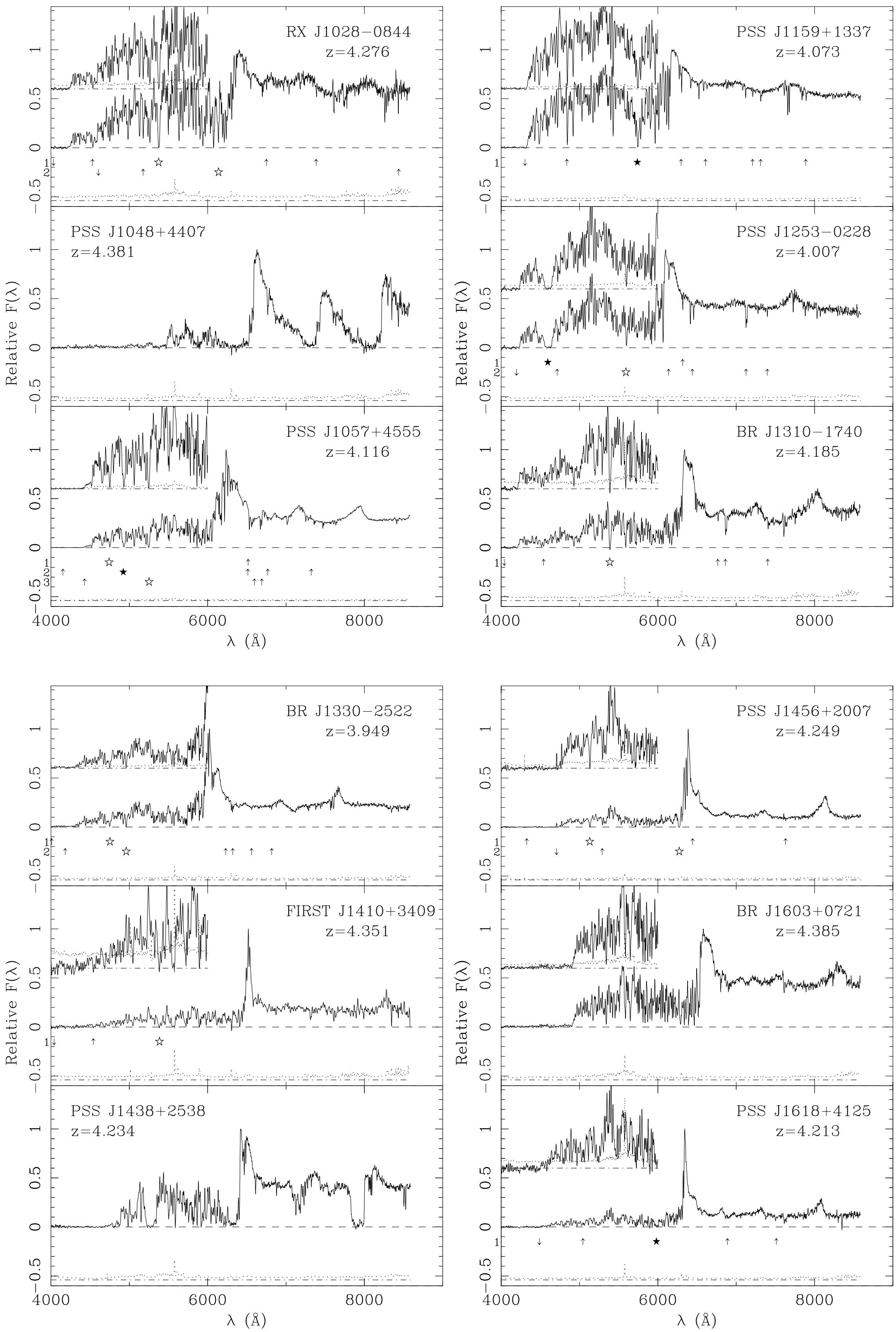

FIG. 1.—*Continued*

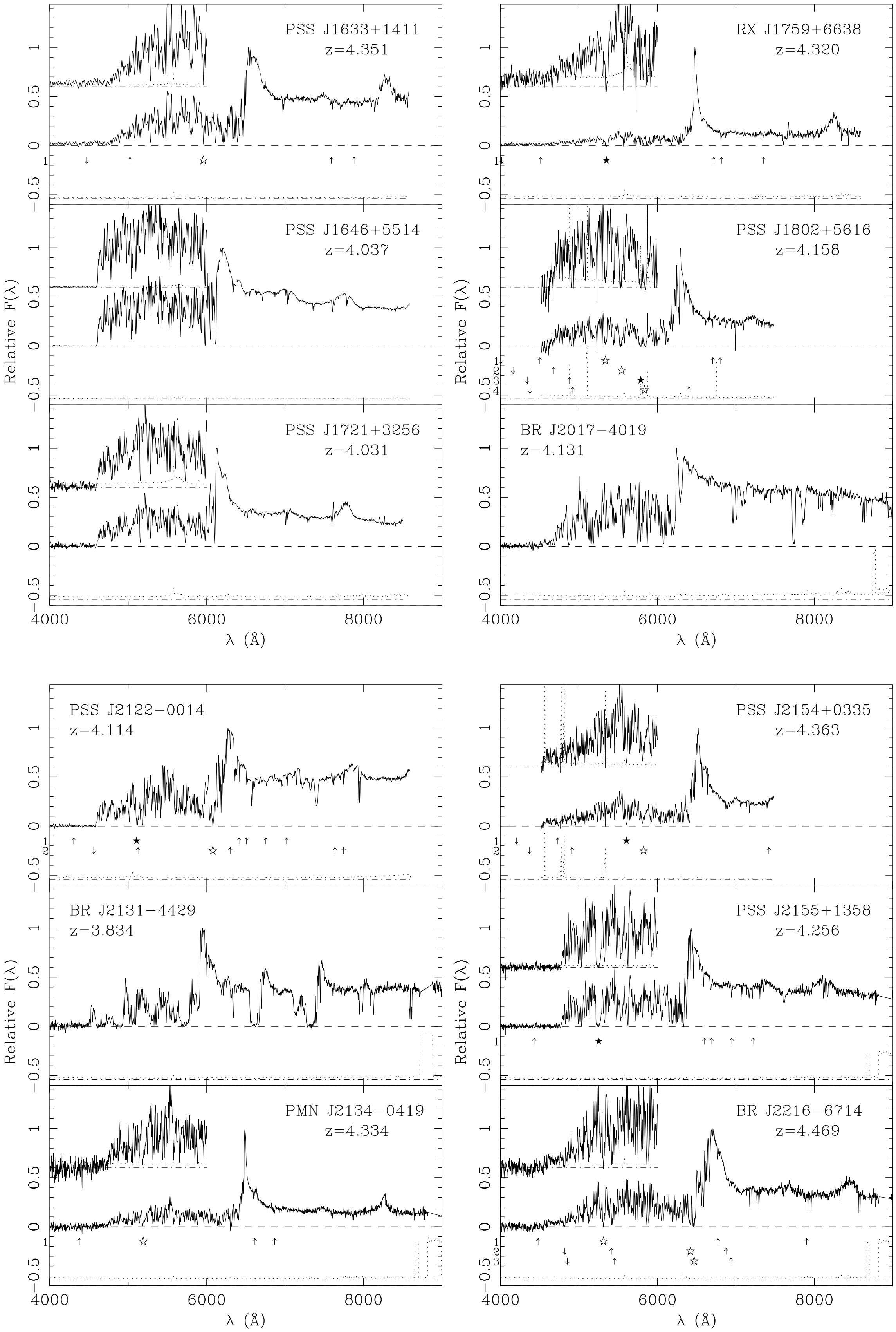

FIG. 1.—*Continued*

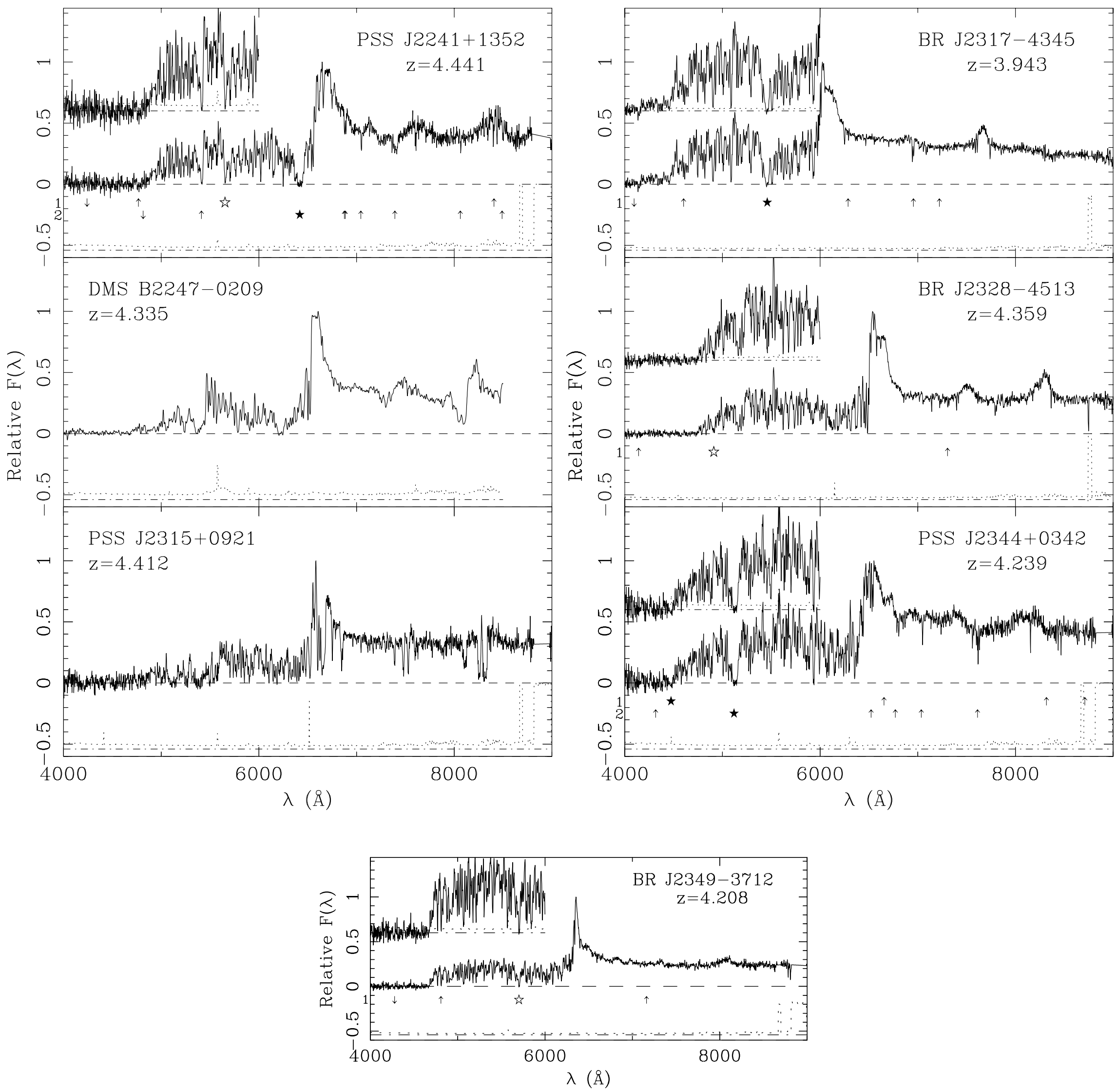

FIG. 1.—*Continued*

TABLE 2

QUASAR REDSHIFT MEASUREMENTS

Quasar	Lyα 1216 Å	N V 1240 Å	O I 1304 Å	Si + O 1400 Å	C IV 1549 Å	Mean Redshift[a]	Note
PSS J0003+2730	4.255	4.205	4.261	4.248	4.233	4.240 ± 0.022	
BR J0006−6208.........	4.505	...	4.471	...	4.388	4.455 ± 0.060	
BR J0030−5129.........	4.163	4.172	4.187	4.175	4.174	4.174 ± 0.009	
PSS J0034+1639	4.309	...	4.298	4.281	4.284	4.293 ± 0.013	
SDSS J0035+0040......	4.737	...	4.758	...	4.746	4.747 ± 0.011	
PSS J0052+2405	...	...	...	...	...	1.90 ± 0.05	BAL,[b]
Q J0054−2742	4.464	...	...	...	...	4.464 ± 0.005	BAL
PSS J0106+2601	4.323	...	4.332	4.303	4.276	4.309 ± 0.025	
PSS J0131+0633	4.431	...	4.430	4.405	4.402	4.417 ± 0.015	
PSS J0133+0400	4.142	...	4.172	4.156	4.148	4.154 ± 0.013	
PSS J0134+3307	4.524	4.534	4.538	4.530	...	4.532 ± 0.006	
PSS J0137+2837	4.297	...	...	...	4.220	4.258 ± 0.054	BAL
PSS J0152+0735	4.042	...	4.064	4.047	4.049	4.051 ± 0.010	
PSS J0207+0940	4.132	...	...	4.142	4.134	4.136 ± 0.005	BAL
PSS J0209+0517	4.174	...	...	...	...	4.174 ± 0.007	
SDSS J0211−0009......	4.874	...	...	...	...	4.874 ± 0.036	
BR J0234−1806.........	4.296	...	...	...	4.307	4.301 ± 0.008	
PSS J0248+1802	4.403	...	4.440	4.428	4.418	4.422 ± 0.016	
BR J0301−5537.........	4.146	...	...	4.125	4.129	4.133 ± 0.011	

TABLE 2—*Continued*

Quasar	Lyα 1216 Å	N V 1240 Å	O I 1304 Å	Si + O 1400 Å	C IV 1549 Å	Mean Redshift[a]	Note
BR J0307−4945	...	...	...	4.738	4.717	4.728 ± 0.015	
SDSS J0310−0014	4.645	4.701	...	4.645	4.639	4.658 ± 0.029	
BR J0311−1722	4.049	4.083	4.025	4.000	...	4.039 ± 0.036	
PSS J0320+0208	3.850	...	...	3.837	3.833	3.840 ± 0.009	BAL
BR J0324−2918	4.609	4.627	4.630	4.615	4.629	4.622 ± 0.009	
BR J0334−1612	4.356	...	4.383	4.364	4.350	4.363 ± 0.014	
SDSS J0338+0021	5.010	...	...	...	...	5.010 ± 0.033	
BR J0355−3811	4.530	...	4.567	4.549	4.533	4.545 ± 0.017	
BR J0403−1703	4.220	4.231	4.232	...	4.227	4.227 ± 0.005	
BR J0415−4357	4.064	...	4.075	4.069	4.072	4.070 ± 0.005	
BR J0419−5716	4.473	...	4.472	4.453	4.445	4.461 ± 0.014	
BR J0426−2202	4.322	4.324	...	4.319	4.314	4.320 ± 0.005	
PMN J0525−3343	4.417	...	...	4.384	4.349	4.383 ± 0.034	
BR J0529−3526	4.411	...	4.419	4.414	4.407	4.413 ± 0.005	
BR J0529−3552	4.172	...	4.181	4.167	4.167	4.172 ± 0.006	
BR J0714−6455	4.483	...	4.486	4.456	4.422	4.462 ± 0.030	
PSS J0747+4434	4.424	4.434	4.442	4.423	4.427	4.430 ± 0.008	
RX J1028−0844	4.235	4.317	...	...	...	4.276 ± 0.058	
PSS J1048+4407	4.422	...	...	4.367	4.354	4.381 ± 0.036	BAL
PSS J1057+4555	4.125	...	...	4.114	4.109	4.116 ± 0.008	
PSS J1159+1337	4.073	...	...	...	...	4.073 ± 0.014	
PSS J1253−0228	4.007	...	...	4.027	3.988	4.007 ± 0.019	
BR J1310−1740	4.201	...	...	4.179	4.175	4.185 ± 0.014	
BR J1330−2522	3.950	3.935	3.961	3.946	3.951	3.949 ± 0.009	
FIRST J1410+3409......	4.357	4.351	4.370	4.338	4.338	4.351 ± 0.014	
PSS J1438+2538	4.275	...	...	4.193	4.232	4.234 ± 0.041	BAL
PSS J1456+2007	4.251	4.255	4.251	4.247	4.242	4.249 ± 0.005	
BR J1603+0721	4.393	...	4.404	...	4.359	4.385 ± 0.024	
PSS J1618+4125	4.212	...	4.220	4.215	4.206	4.213 ± 0.006	
PSS J1633+1411	4.354	...	...	4.347	4.352	4.351 ± 0.004	
PSS J1646+5514	4.071	...	4.058	4.018	4.003	4.037 ± 0.032	
PSS J1721+3256	4.034	...	4.046	4.028	4.016	4.031 ± 0.012	
RX J1759+6638	4.321	4.321	...	4.318	4.318	4.320 ± 0.002	
PSS J1802+5616	4.171	...	...	4.146	...	4.158 ± 0.018	
BR J2017−4019	4.131	...	...	...	...	4.131 ± 0.013	BAL
PSS J2122−0014	4.156	...	...	4.105	4.080	4.114 ± 0.039	
BR J2131−4429	3.871	...	...	3.816	3.814	3.834 ± 0.032	BAL
PMN J2134−0419	4.330	4.344	...	4.331	4.330	4.334 ± 0.007	
PSS J2154+0335	4.360	...	4.367	...	...	4.363 ± 0.005	
PSS J2155+1358	4.285	...	...	4.269	4.216	4.256 ± 0.036	
BR J2216−6714	4.494	...	...	4.467	4.444	4.469 ± 0.025	
PSS J2241+1352	4.419	...	4.469	4.458	4.416	4.441 ± 0.027	
DMS B2247−0209.......	4.378	...	...	4.342	4.284	4.335 ± 0.048	BAL
PSS J2315+0921	4.412	...	...	...	...	4.412 ± 0.041	BAL
BR J2317−4345	3.949	...	...	3.931	3.950	3.943 ± 0.010	
BR J2328−4513	4.366	...	...	4.361	4.349	4.359 ± 0.009	
PSS J2344+0342	...	...	...	...	4.239	4.239 ± 0.052	
BR J2349−3712	4.221	4.169	4.231	...	4.211	4.208 ± 0.028	
median rest-frame composite spectrum	0.002		0.003	−0.001	−0.002	0.001	

NOTE.—BAL: These quasars exhibit broad absorption line characteristics.
[a] The error estimate is $\sigma/\sqrt{n}$.
[b] This object was originally in the PSS web page as a high redshift object. It has since been removed from that list. Our spectrum shows that it is a broad absorption line quasar at $z = 1.9$.

They are defined by a sharp break (due to absorption of photons capable of ionizing H I) shortward of 912 Å. At $z < 1$, LLSs are probably associated with galactic halos (Steidel, Dickinson, & Persson 1994).

Because the search for absorption systems in quasar spectra is not biased toward luminous intervening objects, our data constitute a complementary way to the more traditional emission observations to probe galaxy evolution. The observed number density of LLSs per unit redshift can, for example, be directly compared with models of structure formation (i.e., Abel & Mo 1998). "Gray" LLSs provide some of the best candidates for measurement of the primordial

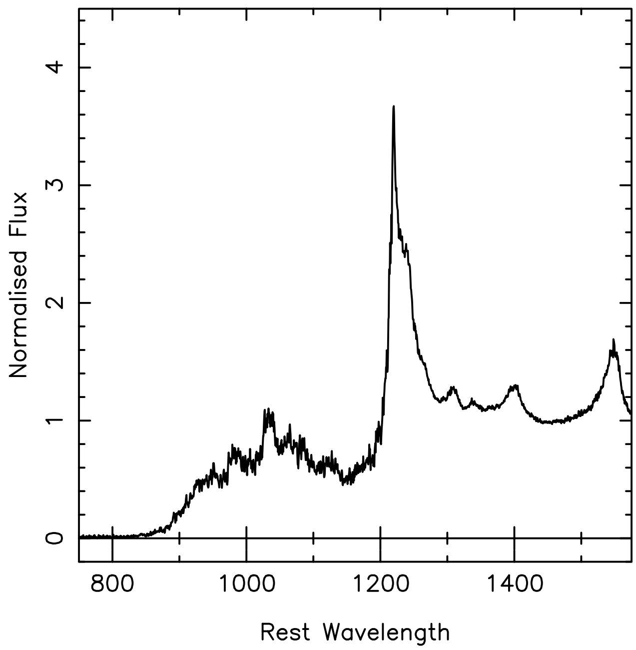

FIG. 2.—Median composite spectrum. This is constructed by correcting each of the non-BAL spectra with enough wavelength coverage to rest frame and normalizing the flux over a region free of emission features (1420–1470 Å).

abundance of deuterium (Molaro et al. 1999; Levshakov, Agafonova, & Kegel 2000 and references herein). Subsequent papers will make use of this new sample of LLSs to constrain their space density, especially at $z \geq 2.4$, where we now have significantly more data than in previous surveys (e.g., Sargent, Steidel, & Boksenberg 1989; Lanzetta et al. 1991; Storrie-Lombardi et al. 1994; Stengler-Larrea et al. 1995).

5.2. *LLS Detection*

The LLSs were identified using an automated technique which determines the ratio (f_+/f_-) of the median of fluxes over 50 Å (rest frame) wide bins slid along the spectrum (see Schneider et al. 1993 for details on this method). The minimum ratio corresponds to a potential LLS detection and the redshift is calculated from the corresponding wavelength. Two examples of the ratio versus LLS redshift plots

TABLE 3

QUASAR MAGNITUDE MEASUREMENTS

Quasars	R^a APM	R^b	Filter[c]	Notes
PSS J0003+2730	18.3	17.8	e	
BR J0006−6208.........	18.3	19.2	R59	
BR J0030−5129.........	18.6	18.6	R59	
PSS J0034+1639	18.0	17.8	e	
SDSS J0035+0040......	...	21.3	e	
PSS J0052+2405	17.4	17.4	e	BAL
Q J0054−2742	19.8	19.8	R59	BAL
PSS J0106+2601	18.5	18.3	e	
PSS J0131+0633	...	19.1	e	NC
PSS J0133+0400	18.3	18.0	e	NC
PSS J0134+3307	19.9	18.9	e	
PSS J0137+2837	18.3	18.6	e	BAL
PSS J0152+0735	18.7	18.0	e	
PSS J0207+0940	18.7	19.2	e	BAL, NC
PSS J0209+0517	17.8	17.8	e	NC
SDSS J0211−0009	...	21.5	e	NC
BR J0234−1806	18.8	19.2	R59	
PSS J0248+1802	17.7	17.6	e	
BR J0301−5537	19.0	18.9	R59	
BR J0307−4945	18.8	18.8	R59	
SDSS J0310−0014	20.7	21.0	R59	NC
BR J0311−1722	17.7	18.0	R59	
PSS J0320+0208	18.5	18.5	e	BAL, NC
BR J0324−2918	18.7	18.6	R59	
BR J0334−1612	17.9	19.2	R59	NC
SDSS J0338+0021	...	21.5	R63	NC
BR J0355−3811	17.9	18.2	R59	
BR J0403−1703	18.7	19.3	R63	NC
BR J0415−4357	18.8	18.9	R59	
BR J0419−5716	17.8	18.7	R59	
BR J0426−2202	17.9	18.0	R59	
PMN J0525−3343	18.4	18.7	R59	
BR J0529−3526	18.9	19.0	R59	
BR J0529−3552	18.3	18.5	R59	
BR J0714−6455	18.3	18.2	R59	
PSS J0747+4434	18.4	19.2	e	NC
RX J1028−0844	18.8	19.1	R59	
PSS J1048+4407	19.6	20.1	e	BAL
PSS J1057+4555	16.5	17.0	e	
PSS J1159+1337	17.1	17.1	e	
PSS J1253−0228	18.8	18.7	R59	
BR J1310−1740	19.5	19.2	R59	
BR J1330−2522	18.5	18.8	R59	
FIRST J1410+3409......	19.9	20.7	e	
PSS J1438+2538	19.3	18.6	e	BAL
PSS J1456+2007	18.2	18.7	e	
BR J1603+0721	19.3	19.4	e	
PSS J1618+4125	18.5	19.0	e	
PSS J1633+1411	18.7	18.2	e	
PSS J1646+5514	17.1	16.5	e	
PSS J1721+3256	18.8	18.1	e	
RX J1759+6638	19.1	19.8	e	
PSS J1802+5616	18.3	19.2	e	NC
BR J2017−4019	18.6	18.2	R59	BAL, NC
PSS J2122−0014	20.3	19.0	R59	NC
BR J2131−4429	18.3	18.4	R59	BAL, NC
PMN J2134−0419	20.0	19.2	R59	
PSS J2154+0335	19.0	18.6	e	NC
PSS J2155+1358	18.0	17.9	e	
BR J2216−6714	18.6	18.6	R59	
PSS J2241+1352	19.1	19.3	e	
DMS B2247−0209.......	19.8	19.0	R63	BAL
PSS J2315+0921	19.2	19.5	e	BAL
BR J2317−4345	19.0	18.5	R59	
BR J2328−4513	19.2	19.1	R59	
PSS J2344+0342	18.2	18.6	e	
BR J2349−3712	18.7	18.7	R59	

NOTES.—The "NC" in the notes column means that the spectrum has not been corrected for slit losses. The BAL designation means the quasar exhibits broad absorption lines.

[a] The R magnitude from the photographic plates as measured by the APM. If no magnitudes are specified in this column, the quasar is not detected on the APM plates. The uncertainties in these magnitudes are estimated to be ± 0.25.

[b] The R magnitude measured from the spectra as described in the text. The uncertainties in these magnitudes are estimated to be ± 0.1.

[c] R59 and R63 are UKST filters, while e is the POSS1 filter.

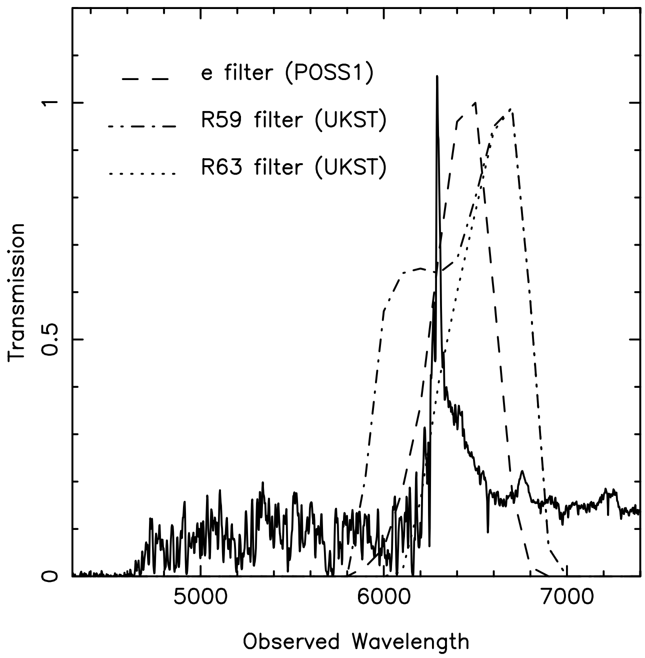

FIG. 3.—Filters used in various surveys. The *R* filters used for the photographic plates scanned with the APM facility are overplotted on the spectrum of $z = 4.172$ BR J0529−3552. The "e" filter was used for the POSS1 survey and the "R59" (R) and "R63" (OR) were used for the UKST survey.

are shown in Figure 4, one for a detection and the other for a nondetection. The optical depth is expressed as the logarithm of the ratio previously defined: $\tau_{\rm LLS} = -\ln(f_+/f_-)$. In some cases, only a fraction of the radiation is absorbed forming a step in the quasar spectra which does not reach zero flux level. These so-called "gray" systems are only taken into account if they have an optical depth, τ, greater than 1. The redshifts and optical depths of the LLSs detected in our sample of quasars are summarized in Table 4, together with the minimum and maximum redshift over which a LLS *could* have been detected. The minimum redshift corresponds to the smallest wavelength in the spectrum and the maximum redshift is 3000 km s^{-1} blueward of the quasar emission redshift. The actual redshift path surveyed is usually limited by the detection of the first Lyman-limit absorber, blueward of which there is either no residual flux or insufficient signal-to-noise to detect further LLSs. The analysis results in the detection of 49 LLSs, 15 of which are within 3000 km s^{-1} of the quasar emission and thus might be associated with the quasar itself. In some cases, metal absorption features are also observed at the redshift of the LLSs.

6. DAMPED Lyα CANDIDATES

6.1. *Background*

Damped Lyα systems have, by definition (Wolfe et al. 1986), a rest-frame equivalent width $W \geq 10$ Å corresponding to $N_{\rm H\,I} \geq 2 \times 10^{20}$ atoms cm^{-2}. At low redshift such high H I column densities are found predominantly in gas-rich systems such as the disks of spiral galaxies. Kinematic studies (such as Prochaska & Wolfe 1998 and Ledoux et al. 1998) and metallicity analyses (such as Pettini et al. 1997 and Prochaska & Wolfe 2000) indicate that DLAs at high redshift might be the progenitors of present day galaxies. Detecting these systems beyond $z \geq 4$ provides observational information about the early stages of galaxy evolution.

DLAs are rare, and to find them requires probing many quasar lines of sight. Figure 5 shows the cumulative number of lines of sight along which a DLA *could* have been detected at the 5 σ confidence level. This survey sensitivity, $g(z)$, is compared with those of previous DLA surveys to show that our new observations more than double the redshift path searched for DLAs at $z \gtrsim 3.5$. Although DLAs

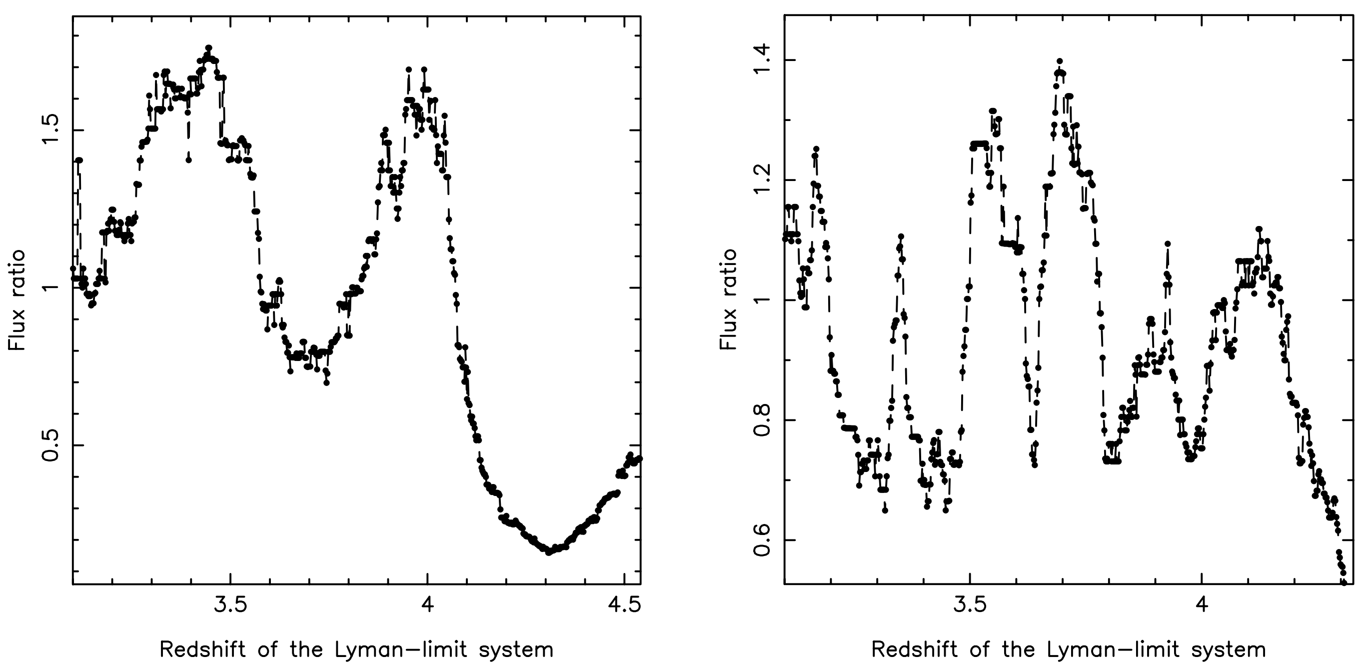

FIG. 4.—LLS detection. Examples of flux ratio above and below the putative Lyman-limit system redshifts. The plot for quasar PSS J2241+1352 (*left panel*) indicates a LLS with redshift $z = 4.31$, while the plot for quasar BR J0403−1703 (*right panel*) does not show the presence of a LLS.

TABLE 4

SURVEY FOR LYMAN-LIMIT SYSTEMS

Quasar	z_{em}	z_{min}[a]	z_{max}[b]	z_{lls}	τ
PSS J0003+2730	4.240	2.858	4.198	3.97	2.6
BR J0006−6208	4.455	3.079	4.400	4.14	1.8
BR J0030−5129	4.174	3.079	4.122	3.37	1.0
PSS J0034+1639	4.293	2.858	4.240	4.26	4.1
SDSS J0035+0040[c]	4.747	3.079	4.690	4.59	0.9
PSS J0106+2601[d]	4.309	2.858	4.256	4.05	2.3
				3.96	2.7
PSS J0131+0633	4.417	3.079	4.363	4.37	2.1
PSS J0133+0400[d]	4.154	3.079	4.102	4.02	1.5
				4.14	2.3
PSS J0134+3307	4.532	2.858	4.477	4.32	2.1
PSS J0152+0735[d]	4.051	2.858	4.000	3.97	2.5
				3.88	2.8
PSS J0209+0517	4.174	3.079	4.122	3.97	2.6
SDSS J0211−0009	4.874	3.079	4.815	4.81	1.2
BR J0234−1806	4.301	3.079	4.248	4.27	2.4
PSS J0248+1802	4.422	2.858	4.368	4.13	2.0
BR J0301−5537	4.133	3.079	4.082	4.10	2.5
BR J0307−4945	4.728	3.079	4.671	4.50	2.8
SDSS J0310−0014[e]	4.658	4.090	4.601	...	...
BR J0311−1722	4.039	3.079	3.989	3.76	2.0
BR J0324−2918	4.622	3.079	4.566	4.21	1.5
BR J0334−1612	4.363	2.858	4.309	4.24	1.4
SDSS J0338+0021	5.010	3.035	4.950	4.93	2.2
BR J0355−3811[d]	4.545	3.079	4.490	4.39	1.6
				4.43	2.0
BR J0403−1703[f]	4.227	4.175	4.175	...	...
BR J0415−4357	4.070	3.079	4.019	4.07	2.6
BR J0419−5716[d]	4.461	3.079	4.406	4.14	1.3
				4.33	1.1
BR J0426−2202[c]	4.320	3.079	4.267	3.97	0.8
PMN J0525−3343	4.383	3.079	4.329	4.09	2.3
BR J0529−3526	4.413	3.079	4.359	4.39	1.7
BR J0529−3552	4.172	3.079	4.120	4.10	2.8
BR J0714−6455	4.462	3.078	4.407	4.46	2.4
PSS J0747+4434	4.430	2.858	4.376	4.29	1.8
RX J1028−0844	4.276	2.857	4.223	3.62	3.0
PSS J1057+4555	4.116	2.857	4.065	3.90	4.4
PSS J1159+1337	4.073	2.857	4.022	3.77	4.0
PSS J1253−0228	4.007	2.857	3.957	3.65	3.5
BR J1310−1740	4.185	2.857	4.133	3.62	2.7
BR J1330−2522[d]	3.949	2.857	3.900	3.72	1.8
				3.82	2.0
FIRST J1410+3409......	4.351	2.857	4.297	3.87	1.2
PSS J1456+2007	4.249	2.857	4.197	4.17	3.5
BR J1603+0721	4.385	2.857	4.331	4.38	2.5
PSS J1618+4125	4.213	2.857	4.161	3.94	2.0
PSS J1633+1411[d]	4.351	2.857	4.297	4.23	1.2
				4.33	1.4
PSS J1646+5514	4.037	2.858	3.987	4.03	5.3
PSS J1721+3256	4.031	2.858	3.981	4.03	2.5
RX J1759+6638[c]	4.320	2.856	4.267	4.20	0.9
PSS J1802+5616[e]	4.158	3.990	4.106	...	...
PSS J2122−0014	4.114	2.858	4.063	4.01	3.5
PMN J2134−0419	4.334	3.079	4.281	4.19	1.6
PSS J2154+0335[e]	4.363	3.990	4.309	...	...
PSS J2155+1358	4.256	3.079	4.203	4.23	2.9
BR J2216−6714	4.469	3.079	4.414	3.98	1.2
PSS J2241+1352	4.441	3.079	4.387	4.31	1.8
BR J2317−4345	3.943	3.079	3.894	3.93	1.4
BR J2328−4513	4.359	3.079	4.305	4.19	2.0
PSS J2344+0342	4.239	3.079	4.187	3.98	1.5
BR J2349−3712	4.208	3.079	4.156	4.17	2.5

[a] z_{min} corresponds to the smallest wavelength in the quasar spectrum.

[b] z_{max} is 3000 km s^{-1} blueward of the quasar emission redshift.

[c] Systems with optical depth, τ, less than 1 are excluded from the total count of LLSs because they do not conform to the formal definition of Lyman-limit Systems.

[d] In case where two breaks were detected, only the highest system is taken into account in the final count for LLSs.

[e] No LLSs have been detected over the specified redshift range.

[f] The signal-to-noise ratio of this spectrum is too low to unable LLS detection.

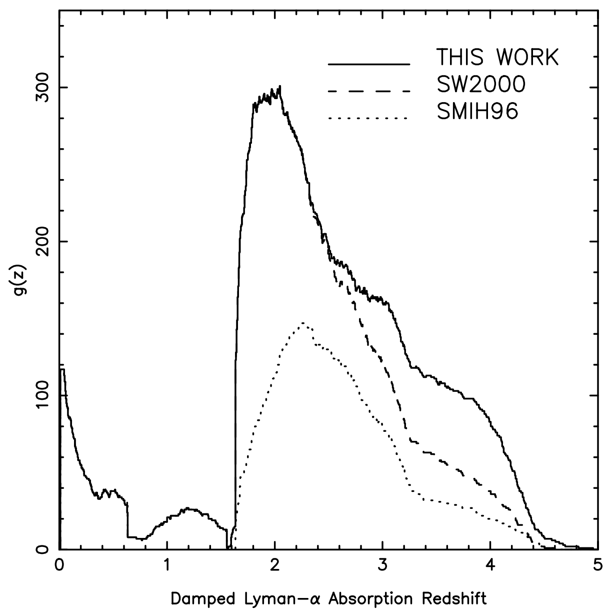

FIG. 5.—Survey sensitivity function. The $g(z)$ function shows the cumulative number of lines of sight along which a DLA system could be detected if there was one. SW00 and SMIH96 are surveys undertaken by Storrie-Lombardi & Wolfe (2000) and Storrie-Lombardi et al. (1996b), respectively. Our new observations more than doubles the redshift path surveyed at $z \geq 3.5$.

have a low number density per unit redshift compared with lower column density systems, they are thought to contain most of the neutral hydrogen mass at $z < 3$. In a subsequent paper (Peroux et al. 2001, in preparation), we will discuss how this new survey impacts upon measurement of the comoving mass density of neutral gas at high redshift, its implications for the formation epoch of DLAs and for the rate of evolution of gas into star.

6.2. *DLA Detection*

To select DLA candidates we have used the detection algorithm following the method developed by Lanzetta et al. (1991), supplemented by a visual search. This has previously been applied to other samples of $z > 4$ quasars in Storrie-Lombardi et al. (1996c) and Storrie-Lombardi & Wolfe (2000). We used the same method for fitting the quasar continua as described in those papers. The spectra were analyzed from 3000 km s^{-1} blueward of the emission line (to avoid lines possibly associated with the quasar) toward shorter wavelengths. The analysis was stopped when the signal-to-noise ratio became too low to detect a Lyα line with rest equivalent width ≥ 5 Å at the 5 σ level (corresponding to z_{min} in Table 5). This point was typically caused by the incidence of a Lyman limit system. We measured the equivalent widths of all the candidates with rest equivalent widths greater than 5 Å and estimated their $N_{\rm H\,I}$ column densities from the linear part of the curve of growth. Previous experience has shown that the column density estimates derived using this method are in good agreement with measurements done on higher resolution data (compare Storrie-Lombardi, Irwin, & McMahon 1996a and Storrie-Lombardi & Wolfe 2000). The results are listed in Table 5. The candidates with rest equivalent widths in the range 5–10 Å at $z \sim 4$ are listed in the table for completion, although they are unlikely to be damped.

TABLE 5

SURVEY FOR DAMPED Lyα ABSORPTION SYSTEMS

Quasar	z_{em}	z_{min}	z_{max}	z_{abs}	W (Å)	log N_{HI} (cm^{-2})	Metal Lines	z_{metal}	Note
PSS J0003+2730	4.240	2.718	4.188	3.51	7.6	20.0	Si II λ1527	3.513	
							Fe II λ1608	3.510	
							Al II λ1671	3.512	
				3.89	9.0	20.2	C II λ1334	3.893	
							Si IV λ1400	3.893	
							C IV λ1549	3.893	
							Al II λ1671	3.891	
BR J0006−6208.........	4.455	2.944	4.400	2.97	15.6	20.7	Si II λ1808	2.965	
				3.20	21.6	20.9	Al II λ1671	3.193	
				3.78	22.5	21.0	Si II λ1527	3.776	
							Fe II λ1608	3.780	a
				4.14	7.9	20.1	C II λ1334	4.150	b
BR J0030−5129.........	4.174	2.304	4.122	2.45	18.1	20.8	Fe II λ2261	2.449	
							Fe II λ2344	2.452	
							Fe II λ2383	2.451	
PSS J0034+1639	4.293	2.981	4.240	3.75	8.9	20.2	Si II λ1527	3.752	
							C IV λ1549	3.754	
				4.26	24.9	21.1	Si II λ1260	4.252	b,c
							O I λ1302	4.262	
							C II λ1334	4.282	
							Si IV λ1400	4.281	
							Si II λ1527	4.282	
							C IV λ1549	4.281	
							Fe II λ1608	4.281	
SDSS J0035+0040......	4.747	3.309	4.690	...	...	...	...	...	
PSS J0106+2601	4.309	2.764	4.256	3.96	13.5	20.5	Lyβ	3.96	b
							C II λ1334	3.958	
							Si IV λ1400	3.957	
							C IV λ1549	3.959	
PSS J0131+0633	4.417	3.014	4.363	3.17	6.6	19.9	...	...	
				3.61	5.5	19.8	C IV λ1549	3.609	
PSS J0133+0400	4.154	2.865	4.102	3.08	8.2	20.1	C IV λ1549	3.083	
							Si II λ1808	3.085	
				3.69	11.9	20.4	Si II λ1527	3.691	
							Al II λ1671	3.690	
				3.77	12.5	20.5	C II λ1334	3.771	
							Si IV λ1400	3.771	
							Si II λ1527	3.771	
							Fe II λ1608	3.770	
							Al II λ1671	3.771	
				4.00	8.6	20.1	Si II λ1260	3.993	
							O I λ1302	3.994	
							Si IV λ1400	3.996	
							Si II λ1527	3.993	
PSS J0134+3307	4.532	2.562	4.477	3.76	14.8	20.6	Si II λ1527	3.761	d
							C IV λ1549	3.775	
							Al II λ1671	3.780	
PSS J0152+0735	4.051	1.890	4.000	3.84	17.0	20.7	Lyβ	3.84	b
							O I λ1302	3.841	
							C II λ1334	3.842	
PSS J0209+0517	4.174	2.759	4.122	3.66	10.1	20.3	Al II λ1671	3.664	
				3.86	15.2	20.6	Lyβ	3.86	
							Si II λ1304	3.862	
							C II λ1334	3.862	
SDSS J0211−0009......	4.874	3.402	4.815	4.64	7.5	20.0	Si II λ1527	4.645	
BR J0234−1806.........	4.301	2.971	4.248	3.69	8.7	20.2	Si IV λ1400	3.694	
							Al II λ1671	3.692	
PSS J0248+1802	4.422	2.810	4.368	...	...	...	...	...	
BR J0301−5537.........	4.133	2.825	4.082	3.22	10.4	20.3	Si II λ1527	3.220	
				3.38	7.9	20.1	Si II λ1527	3.377	
				3.71	7.0	20.0	C II λ1334	3.705	
							C IV λ1549	3.701	
BR J0307−4945.........	4.728	3.138	4.671	3.35	6.0	19.8	...	...	
				4.46	18.6	20.8	Lyβ	4.46	b
							O I λ1302	4.465	
							Si II λ1304	4.466	
							C II λ1334	4.465	
							Si IV λ1400	4.464	
							Si II λ1527	4.466	
							C IV λ1549	4.464	

TABLE 5—*Continued*

Quasar	z_{em}	z_{min}	z_{max}	z_{abs}	W (Å)	log $N_{H\,I}$ (cm^{-2})	Metal Lines	z_{metal}	Note
							Fe II λ1608	4.466	
							Al II λ1671	4.466	
SDSS J0310−0014	4.658	3.087	4.601	3.42	13.2	20.5	Al II λ1671	3.424	
				4.34	8.6	20.1	...	...	
BR J0311−1722	4.039	2.591	3.989	3.73	8.7	20.2	O I λ1302	3.733	
							Si II λ1304	3.733	
							C II λ1334	3.733	
BR J0324−2918	4.622	2.900	4.566	...	...	...	...	...	
BR J0334−1612	4.363	3.080	4.309	3.56	24.5	21.0	Si II λ1527	3.558	
SDSS J0338+0021	5.010	3.528	4.950	4.06	11.8	20.4	Si II λ1527	4.059	
							Al II λ1671	4.066	
BR J0355−3811	4.545	3.030	4.490	...	...	...	...	...	
BR J0403−1703	4.227	2.992	4.175	...	...	...	...	...	
BR J0415−4357	4.070	2.813	4.019	3.81	7.1	20.1	Lyβ	3.81	
							O I λ1302	3.806	
							Si II λ1304	3.806	
							C II λ1334	3.806	
							Si II λ1527	3.806	
BR J0419−5716	4.461	2.820	4.406	2.82	7.4	20.0	Fe II λ2344	2.819	
				2.90	8.8	20.2	Fe II λ2344	2.896	
				2.98	5.1	19.7	...	...	
BR J0426−2202	4.320	2.544	4.267	2.98	26.2	21.1	Al II λ1671	2.982	
PMN J0525−3343	4.383	2.829	4.329	...	...	...	...	...	
BR J0529−3526	4.413	3.023	4.359	3.57	8.5	20.1	Fe II λ1608	3.573	
							Al II λ1671	3.571	
BR J0529−3552	4.172	2.821	4.120	3.68	7.6	20.0	...	...	
				3.70	7.6	20.0	...	...	
BR J0714−6455	4.462	3.050	4.407	...	...	...	...	...	
PSS J0747+4434	4.430	2.764	4.376	3.76	10.3	20.3	...	...	
				4.02	15.4	20.6	Lyβ	4.02	
							C II λ1334	4.020	
							Al II λ1671	4.017	
RX J1028−0844	4.276	2.533	4.223	3.42	8.0	20.1	Lyβ	3.422	
							Si II λ1527	3.423	
							Al II λ1671	3.422	
				4.05	5.0	19.7	Al II λ1671	4.047	e
PSS J1057+4555	4.116	2.652	4.065	2.90	8.0	20.1	Al II λ1671	2.910	
				3.05	10.0	20.3	Fe II λ1608	3.061	
							Al II λ1671	3.051	
							Si II λ1808	3.049	
				3.32	8.9	20.2	Si II λ1527	3.316	
							Al II λ1671	3.317	
PSS J1159+1337	4.073	2.563	4.022	3.72	10.3	20.3	Lyβ	3.72	b,f
							C II λ1334	3.723	
							Si IV λ1400	3.723	
							Si II λ1527	3.723	
							C IV λ1549	3.724	
							Al II λ1671	3.723	
PSS J1253−0228	4.007	2.498	3.957	2.78	38.5	21.4	Al II λ1671	2.781	b
				3.60	5.2	19.7	C II λ1334	3.602	
							Si IV λ1400	3.603	
							C IV λ1549	3.602	
							Fe II λ1608	3.599	
BR J1310−1740	4.185	2.508	4.133	3.43	8.1	20.1	Si II λ1527	3.435	
							C IV λ1549	3.434	
							Al II λ1671	3.433	
BR J1330−2522	3.949	2.578	3.900	2.91	7.5	20.0	...	...	
				3.08	5.7	19.8	Si II λ1527	3.082	
							C IV λ1549	3.081	
							Fe II λ1608	3.080	
							Al II λ1671	3.080	
FIRST J1410+3409......	4.351	3.026	3.578	3.43	8.2	20.1	...	...	
		3.602	4.297	...	...	...	...	...	
PSS J1456+2007	4.249	2.878	4.197	3.22	5.6	19.8	Si II λ1527	3.223	
							Si II λ1808	3.221	
				4.16	6.8	19.9	...	...	b
BR J1603+0721	4.385	3.062	4.331	...	...	...	...	...	
PSS J1618+4125	4.213	2.820	4.161	3.92	12.9	20.5	Si IV λ1400	3.920	b
							Si II λ1527	3.914	

TABLE 5—*Continued*

Quasar	z_{em}	z_{min}	z_{max}	z_{abs}	W (Å)	log $N_{H\,I}$ (cm^{-2})	Metal Lines	z_{metal}	Note
PSS J1633+1411	4.351	2.536	4.297	3.90	5.8	19.8	C IV λ1549	3.895	
							Fe II λ1608	3.906	
PSS J1646+5514	4.037	2.772	3.987	...	...	...	...	...	
PSS J1721+3256	4.031	2.791	3.981	...	...	...	...	...	
RX J1759+6638	4.320	2.804	4.267	3.40	12.4	20.4	Si II λ1527	3.398	
							C IV λ1549	3.397	
							Al II λ1671	3.397	
PSS J1802+5616	4.158	2.891	4.106	3.39	8.3	20.1	Si II λ1527	3.386	
							C IV λ1549	3.389	
				3.56	9.7	20.2	...	...	
				3.76	11.2	20.4	...	...	
				3.80	8.5	20.1	C II λ1334	3.807	
PSS J2122−0014	4.114	2.350	4.063	3.20	10.7	20.3	Si II λ1527	3.206	g
							C IV λ1549	3.206	
							Fe II λ1608	3.205	
							Al II λ1671	3.206	
				4.00	8.0	20.1	Si II λ1260	3.999	b
							Si II λ1527	4.001	
							C IV λ1549	4.000	
PMN J2134−0419......	4.334	2.903	4.281	3.27	7.0	20.0	C IV λ1549	3.262	
							Fe II λ1608	3.269	
PSS J2154+0335	4.363	2.979	4.309	3.61	11.3	20.4	Si II λ1527	3.623	
				3.79	5.4	19.7	C IV λ1549	3.778	
PSS J2155+1358	4.256	2.940	4.203	3.32	24.6	21.1	Si II λ1527	3.316	h
							C IV λ1549	3.313	
							Fe II λ1608	3.316	
							Al II λ1671	3.314	
BR J2216−6714.........	4.469	2.795	4.414	3.37	7.0	20.0	C IV λ1549	3.369	
							Si II λ1808	3.364	
				4.28	7.0	20.0	Lyβ	4.28	
							O I λ1302	4.262	
				4.32	8.3	20.1	Si II λ1304	4.323	
PSS J2241+1352	4.441	3.027	4.387	3.65	7.2	20.0	Si II λ1808	3.647	
				4.28	17.1	20.7	Lyβ	4.28	
							O I λ1302	4.282	
							Si II λ1304	4.284	
							C II λ1334	4.282	
							Si IV λ1400	4.286	
							Si II λ1527	4.283	
							Fe II λ1608	4.284	
BR J2317−4345.........	3.943	2.448	3.894	3.49	20.2	20.9	Si IV λ1400	3.483	
							C IV λ1549	3.486	
							Fe II λ1608	3.491	
BR J2328−4513.........	4.359	2.926	4.305	3.04	8.3	20.1	Si II λ1808	3.041	i
PSS J2344+0342	4.239	2.696	4.187	2.68	23.0	21.0	Si II λ1808	2.678	j
							Fe II λ2260	2.684	
							Fe II λ2367	2.678	
				3.21	21.1	20.9	C IV λ1549	3.218	
							Fe II λ1608	3.219	
							Al II λ1671	3.219	
							Si II λ1808	3.220	
BR J2349−3712.........	4.208	2.847	4.156	3.69	9.5	20.2	Si II λ1527	3.691	

[a] Fe II λ1608 at $z = 3.780$ is at the same position as Fe II λ2600 at $z = 1.958$.

[b] Also detected as a Lyman-limit system.

[c] This damped system is within 3000 km s^{-1} of the quasar emission redshift but we have included it in this table due to the fact that it is the first damped absorber detected at a redshift $z > 4$ with a column density log $N_{H\,I} > 21$.

[d] Si II λ1527 at $z = 3.761$ is at the same position as C IV λ1549 at $z = 3.686$.

[e] Al II λ1671 at $z = 4.047$ is at the same position as Mg I λ2853 at $z = 1.956$.

[f] This damped absorption line has a very narrow core, but strong damping wings are visible on both sides of the line.

[g] The Lyα line may be blended with Lyβ at $z = 4.00$, therefore the column density may be overestimated. This quasar has an unusually rich absorption spectrum, with many C IV absorbers redward of the Lyα emission.

[h] Si II λ1527 at $z = 3.316$ is at the same position as Fe II λ2260 at $z = 1.915$.

[i] Si II λ1808 at $z = 3.041$ is blended with C IV λ1549 at $z = 3.719$.

[j] This damped absorption candidate is just below the minimum redshift determined with our detection algorithm. It is likely to be real but requires confirmation with a higher signal-to-noise spectrum.

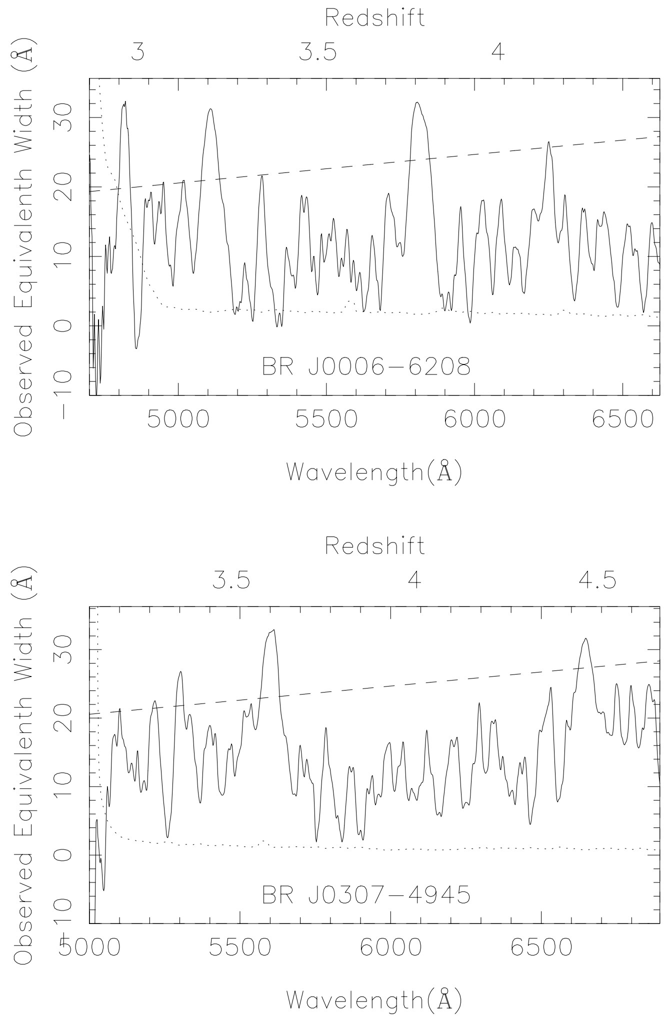

FIG. 6.—DLA detection. The figure shows two examples of the output from the algorithm that detects damped Lyα absorption candidates. The spectrum equivalent width bins are shown as a solid line, the error equivalent width bins are shown as a dotted line, and the dashed line shows the observed equivalent width of a 5 Å rest equivalent width line at the redshifts shown along the top axis. The lower axis shows the wavelength scale. The minimum redshift ($z_{\rm min}$ in Table 5) to which we can survey for damped candidates is determined by the point where the error line (*dotted*) crosses the 5 Å rest equivalent width threshold (*dashed line*). The places where the spectrum array (*solid line*) goes above the dashed line threshold are the wavelengths at which we measure the equivalent width of the lines in the original spectrum. The upper panel shows four potential absorbers in BR J0006−6208, and the lower panel shows five potential absorbers in BR J0307−4945.

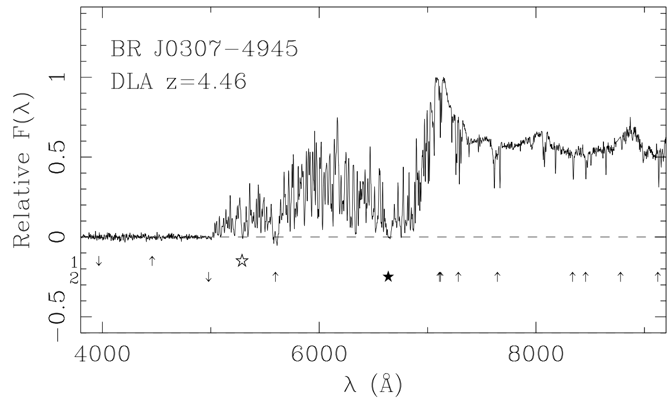

FIG. 7.—Example of DLA candidates. The spectrum of quasar BR J0307−4945 with DLA candidates marked at $z = 4.46$ and $z = 3.35$ is shown. The $z = 4.46$ absorber is the highest redshift damped absorber currently detected. The notations are as in Fig. 1. Many metal lines are observed at $z = 4.46$, but no metals are detected at $z = 3.35$. The higher redshift DLA has been studied in detail with higher resolution observations undertaken with the UVES spectrograph (Dessauges-Zavadsky et al. 2000).

Figure 6 shows two examples (BR J0006−6208 and BR J0307−4945) of the output of the algorithm we use to detect DLA candidates. The highest redshift ($z = 4.46$) DLA system currently known is detected in the spectrum of quasar BR J0307−4945 (Fig. 7). It has many associated metal lines which have been studied in detail with higher resolution observations undertaken with the UVES spectrograph (Dessauges-Zavadsky et al. 2000).

6.3. *Metal Lines in the DLAs*

Absorption features redward of the Lyα quasar emission line were selected using an automated algorithm[2] developed by Bob Carswell. The code systematically detects lines with equivalent width $W \geq 0.1$ Å. Gaussians were fitted to the lines in order to measure their redshifts and equivalent widths. Some of these lines were identified as low-ionization states of metals in association with DLA candidates. In some cases Lyβ was observed blueward of the DLA candidate. All the metal lines associated with DLA candidates are listed in Table 5.

7. METAL SYSTEMS

The observed equivalent width and wavelength of every absorption line detected redward of the quasar Lyα emis-

TABLE 6

METAL LINES REST WAVELENGTHS

Ion	λ (Å)	Reference
N V	1238.821	1
N V	1242.804	1
Si II	1260.4221	1
Si II	1304.3702	1
C II	1334.5323	1
Si IV	1393.7550	1
Si IV	1402.7700	1
Si II	1526.7066	1
C IV	1548.1950	1
C IV	1550.7700	1
Fe II	1608.4511	1
Fe II	1611.2005	1
Al II	1670.7874	1
Si II	1808.0126	2
Fe II	2260.7805	1
Fe II	2344.2140	1
Fe II	2367.5910	3
Fe II	2374.4612	4
Fe II	2382.7650	4
Fe II	2586.6500	4
Fe II	2600.1729	4
Mg II	2796.3520	1
Mg II	2803.5310	1
Mg I	2852.9641	1

REFERENCES.—(1) Morton 1991; (2) Bergeson & Lawler 1993; (3) Nussbaumer et al. 1982; (4) Cardelli et al. 1995.

TABLE 7

Identification of Metal Absorption Lines

Quasar	z_{em}	λ_{obs} (Å)	W_{obs} (Å)	Ion	λ_{rest} (Å)	z
PSS J0003+2730...	4.240	6530.3	5.6	C II	1334	3.893
		6819.2	2.1	Si IV	1393	3.893
		6863.6	1.6	Si IV	1402	3.893
		6889.8	1.4	Si II	1527	3.513
		7254.7	1.7	Fe II	1608	3.510

Note.—Table 7 is available in its entirety in the electronic edition of the Astronomical Journal. A portion is shown here for guidance regarding its form and content

sion were measured using the algorithm described in § 6.3 above. The features which were not associated with a DLA or LLSs were identified using the line list in Table 6. Most of the detected Mg II systems also show associated Fe II absorption. This survey resulted in the detection of 80 new C IV systems ($3.0 \lesssim z \lesssim 4.5$) and 48 new Mg II systems ($1.3 \lesssim z \lesssim 2.2$). The results are summarized in Table 7.

8. NOTES ON INDIVIDUAL OBJECTS

1. *PSS J0003+2730* ($z = 4.240$).—This quasar has two weak Lyα absorbers at $z = 3.51$ and 3.89. Neither has an estimated column density greater than $10^{20.3}$ atoms cm^{-2}, but metal lines associated with both absorbers have been detected.

2. *BR J0006−6208* ($z = 4.455$): This quasar has weak emission lines but a rich absorption spectrum. There are four candidate damped absorbers at $z = 2.97$, 3.20, 3.78, and 4.14. The highest redshift is a weak candidate, but the other three all have high estimated column densities. All the candidates have at least one associated metal absorption line. In addition, there is a Mg II absorption system at $z = 1.958$.

3. *BR J0030−5129* ($z = 4.174$).—This quasar has one candidate damped absorber at $z = 2.45$ with three associated Fe II lines.

4. *PSS J0034+1639* ($z = 4.293$).—This quasar has two damped Lyα candidate absorbers. The first is at $z = 3.75$ and the estimated column density of log $N_{\rm H\,I} = 20.2$ falls just below the formal definition of DLAs. Associated Si II and C IV metal lines are detected. The second damped system is at $z = 4.26$ which is within 3000 km s^{-1} of the emission redshift of the quasar ($z = 4.293$) so it will not be included as an intervening absorber in the statistical samples used in determining the neutral gas mass. However, it is of interest because this is the first damped system detected at a redshift greater than 4 with a column density log $N_{\rm H\,I} > 21$. We estimate the column density for this system at log $N_{\rm H\,I} = 21.1$ and detected associated metals lines of Si II, O I, C II, Si IV, C IV, and Fe II in the range $z = 4.252$–4.282.

5. *SDSS J0035+0040* ($z = 4.747$).—We detect no damped Lyα candidates in this spectrum. This is one of the lower signal-to-noise spectra in our sample due to the faintness of the quasar ($R = 21.3$), but we would have been able to detect a DLA with a column density log $N_{\rm H\,I} \geq 20.3$ over the redshift range $3.309 < z < 4.690$.

6. *PSS J0052+2405* ($z = 1.90$).—This is a broad absorption lines quasar at $z = 1.9$. We observed it because the coordinates were originally in the list of PSS $z > 4$ quasars available at their web site.[3] It has since been removed from that list.

7. *Q J0054−2742* ($z = 4.464$).—This quasar exhibits broad absorption lines. The spectrum is not used in our absorption line survey.

8. *PSS J0106+2601* ($z = 4.309$).—This quasar has a strong candidate damped absorber at $z = 3.96$ with associated metal lines.

9. *PSS J0131+0633* ($z = 4.417$).—This quasar has two very weak candidate damped absorbers at $z = 3.17$ and 3.69. C IV is also detected at $z = 3.69$.

10. *PSS J0133+0400* ($z = 4.154$).—This spectrum has four candidate damped absorbers. The absorbers at $z = 3.69$ and 3.77 have estimated column densities above the formal definition of DLA ($N_{\rm H\,I} \geq 10^{20.3}$ atoms cm^{-2}), and the absorbers at $z = 3.08$ and 4.00 are below that threshold. Associated metal lines are detected for all of the candidate DLAs.

11. *PSS J0134+3307* ($z = 4.532$).—The quasar has a DLA at $z = 3.76$ with associated metal lines.

12. *PSS J0137+2837* ($z = 4.258$).—This quasar exhibits broad absorption lines. The spectrum is not used in our absorption line survey.

13. *PSS J0152+0735* ($z = 4.051$).—This quasar has an excellent DLA candidate at $z = 3.84$ with associated metal lines, which is also detected as a Lyman limit system.

14. *PSS J0207+0940* ($z = 4.136$).—This quasar exhibits strong intrinsic absorption features. The spectrum is not used in our absorption line survey.

15. *PSS J0209+0517* ($z = 4.174$).—This quasar has weak emission lines but exhibits two DLA candidates at $z = 3.66$ and 3.86. Both have associated metal absorption features.

16. *SDSS J0211−0009* ($z = 4.874$).—We detect one weak candidate DLA in this quasar at $z = 4.64$. Si II is also detected at that redshift.

17. *BR J0234−1806* ($z = 4.301$).—This quasar shows one weak absorption candidate at $z = 3.69$ with associated metal lines.

18. *PSS J0248+1802* ($z = 4.422$).—This spectrum shows no DLA candidates.

19. *BR J0301−5537* ($z = 4.133$).—This quasar shows three DLA candidates at $z = 3.22$, 3.38, and 3.71. All have associated metal lines, but the two higher redshift candidates have estimated column densities below 2×10^{20} atoms cm^{-2}.

20. *BR J0307−4945* ($z = 4.728$).—The spectrum shows the highest redshift damped absorber currently known at $z = 4.46$ with an estimated column density of log $N_{\rm H\,I} =$ 20.8. Associated metal lines of Si II, O I, C II, Si IV, C IV, Fe II, and Al II are also detected at this redshift. The spectrum is shown in Figure 7. The spectrum of this object is discussed in more detail in McMahon et al. (2001, in preparation) and Dessauges-Zavadsky et al. (2000). There is a weak DLA

[2] See the following URL for more details: http://www.ast.cam.ac.uk/~rfc/rdgen.html.

[3] http://www.astro.caltech.edu/~george/z4.qsos.

candidate at $z = 3.35$ with no associated metal lines. This absorber is highly unlikely to be damped.

21. *SDSS J0310−0014* ($z = 4.658$).—This quasar shows two candidate DLAs at $z = 3.42$ and 4.34. The lower redshift system has an estimated column density above the DLA threshold. An associated Al II line is detected at $z = 3.424$, but no metal lines associated with the higher redshift candidate are detected.

22. *BR J0311−1722* ($z = 4.039$).—This quasar has a weak DLA candidate at $z = 3.73$ which is also detected as a Lyman-limit system. Associated metal lines are also detected.

23. *PSS J0320+0208* ($z = 3.840$).—This quasar exhibits broad absorption lines. The spectrum is not used in our absorption line survey.

24. *BR J0324−2918* ($z = 4.622$).—No DLA candidates are detected in this spectrum.

25. *BR J0334−1612* ($z = 4.363$).—A DLA candidate at $z = 3.56$ with associated Si II is detected in this quasar. This candidate has previously been detected (Storrie-Lombardi & Wolfe 2000) with a lower estimated column density (log $N_{\rm H\,I} = 20.6$) than we measure.

26. *SDSS J0338+0021* ($z = 5.010$).—This quasar has one DLA candidate at $z = 4.06$ with associated metals detected.

27. *BR J0355−3811* ($z = 4.545$).—No DLA candidates are detected in this spectrum. There is a Mg II absorber at $z = 2.228$.

28. *BR J0403−1703* ($z = 4.227$).—No DLA candidates are detected. No metal lines could be identified in this spectrum.

29. *BR J0415−4357* ($z = 4.070$).—A weak DLA candidate with associated metal lines is detected at $z = 3.81$.

30. *BR J0419−5716* ($z = 4.461$).—Three weak DLA candidates are detected just above the Lyman-limit edge in this spectrum at $z = 2.82$, 2.90, and 2.98. One associated metal line is detected from each of the two lower redshift systems.

31. *BR J0426−2202* ($z = 4.320$).—A very high column density candidate (log $N_{\rm H\,I} = 21.1$) is detected at $z = 2.98$ with associated Al II.

32. *PMN J0525−3343* ($z = 4.383$).—No DLA candidates are detected in this spectrum. Two Mg II absorbers are detected at $z = 1.570$ and 2.006.

33. *BR J0529−3526* ($z = 4.413$).—A weak DLA candidate with associated metal lines is detected at $z = 3.57$.

34. *BR J0529−3552* ($z = 4.172$).—A "doublet" of weak DLA candidates is detected at $z = 3.68$ and 3.70. No associated metals are detected at these redshifts.

35. *BR J0714−6455* ($z = 4.462$).—No DLA candidates are detected in this spectrum.

36. *PSS J0747+4434* ($z = 4.430$).—Two DLA candidates are detected at $z = 3.76$ and 4.02. The higher redshift system also has associated metal lines.

37. *RX J1028−0844* ($z = 4.276$).—Two weak DLA candidates with associated metals are detected at $z = 3.42$ and 4.05.

38. *PSS J1048+4407* ($z = 4.381$).—This quasar exhibits broad absorption lines. The spectrum is not used in our absorption line survey.

39. *PSS J1057+4555* ($z = 4.116$).—Three DLA candidates are detected at $z = 2.90$, 3.05, and 3.32. The candidate absorber at $z = 3.32$ has been confirmed as damped in a higher resolution spectrum. It has a redshift of $z = 3.3172$ and a column density log $N_{\rm H\,I} = 20.34$ (Lu, Sargent, & Barlow 1998). The estimated column density (log $N_{\rm H\,I} = 20.3$) for the $z = 3.05$ is identical to the estimate reported in Storrie-Lombardi & Wolfe (2000).

40. *PSS J1159+1337* ($z = 4.073$).—This quasar has a DLA candidate at $z = 3.72$ with several associated metal lines.

41. *PSS J1253−0228* ($z = 4.007$).—This quasar has two candidate damped absorbers. One absorber at $z = 2.78$ has a very high estimated column density (log $N_{\rm H\,I} = 21.4$), and an associated Al II line is detected. This is the highest column density absorber in our survey. Another absorber at $z = 3.60$ is highly unlikely to be damped, with an estimated column density of log $N_{\rm H\,I} = 19.7$, but does have several associated metal lines.

42. *BR J1310−1740* ($z = 4.185$).—This quasar has a weak damped candidate at $z = 3.43$. Associated metal lines are also detected at this redshift.

43. *BR J1330−2522* ($z = 3.949$).—This quasar has two weak DLA candidates at $z = 2.91$ and 3.08. The higher redshift system has associated metal lines.

44. *FIRST J1410+3409* ($z = 4.351$).—There is a weak candidate damped absorber at $z = 3.43$ with no associated metal lines. In this spectrum the redshift path surveyed for damped absorbers is not continuous due to a large noise spike in the forest at $z \approx 3.59$.

45. *PSS J1438+2538* ($z = 4.234$).—This quasar exhibits broad absorption lines. The spectrum is not used in our absorption line survey.

46. *PSS J1456+2007* ($z = 4.249$).—There are two weak DLA candidates at $z = 3.22$ and 4.16. The lower redshift system also has associated metal lines.

47. *BR J1603+0721* ($z = 4.385$).—No DLA candidates are detected in this spectrum.

48. *PSS J1618+4125* ($z = 4.213$).—There is a DLA candidate at $z = 3.92$ with associated metal lines.

49. *PSS J1633+1411* ($z = 4.351$).—There is a weak DLA candidate at $z = 3.90$ with associated metal lines.

50. *PSS J1646+5514* ($z = 4.037$).—No DLA candidates are detected in this spectrum.

51. *PSS J1721+3256* ($z = 4.031$).—No DLA candidates are detected in this spectrum.

52. *RX J1759+6638* ($z = 4.320$).—There is a DLA candidate at $z = 3.40$ with associated metal lines.

53. *PSS J1802+5616* ($z = 4.158$).—There are four damped absorber candidates detected in this spectrum at $z = 3.39$, 3.56, 3.76, and 3.80. Only the absorber at $z = 3.76$ has an estimated column density above the formal definition of DLA ($N_{\rm H\,I} \geq 10^{20.3}$ atoms cm^{-2}). Associated metal lines are detected for the $z = 3.39$ and 3.80 absorbers.

54. *BR J2017−4019* ($z = 4.131$).—This quasar exhibits strong intrinsic absorption at the quasar emission redshift. The C IV and Si IV emission lines are completely absorbed. The spectrum is not used in our absorption line survey.

55. *PSS J2122−0014* ($z = 4.114$).—This spectrum shows two DLA candidates at $z = 3.20$ and 4.00. We estimate the column density of the lower redshift system to be log $N_{\rm H\,I} = 20.3$, but this may be an overestimating as the Lyα line at $z = 3.20$ is at the same position as the Lyβ line at $z = 4.00$. Associated metal lines are detected for both absorption systems.

56. *BR J2131−4429* ($z = 3.834$).—This quasar exhibits broad absorption lines. The spectrum is not used in our absorption line survey.

57. *PMN J2134−0419* ($z = 4.334$).—This quasar has one weak DLA candidate at $z = 3.27$ with associated metal lines.

58. *PSS J2154+0335* ($z = 4.363$).—This quasar has two DLA candidates at $z = 3.61$ and 3.79. Metal lines are detected for both, but only the lower redshift system has an estimated column density above 2×10^{20} atoms cm^{-2}.

59. *PSS J2155+1358* ($z = 4.256$).—This quasar has a very high column density (log $N_{\rm H\,I} = 21.1$) DLA candidate at $z = 3.32$. Associated metal lines are also detected at this redshift.

60. *BR J2216−6714* ($z = 4.469$).—This quasar has three weak DLA candidates at $z = 3.27$, 4.28, and 4.32. At least one associated metal line has been detected for each.

61. *PSS J2241+1352* ($z = 4.441$).—This quasar has two DLA candidates at $z = 3.65$ and 4.28. The lower redshift system has an estimated column density below the formal definition of DLA ($N_{\rm H\,I} \geq 10^{20.3}$ atoms cm^{-2}). Both have associated metal lines.

62. *DMS B2247−0209* ($z = 4.335$).—This quasar exhibits broad absorption lines. The spectrum is not used in our absorption line survey.

63. *PSS J2315+0921* ($z = 4.412$).—This quasar exhibits strong intrinsic absorption at the quasar emission redshift. The C IV and Si IV emission lines are almost completely absorbed. It is similar in character to the spectrum of BR J2017−4019. The spectrum is not used in our absorption line survey.

64. *BR J2317−4345* ($z = 3.943$).—This quasar has a strong DLA candidate at $z = 3.49$ with associated metal lines.

65. *BR J2328−4513* ($z = 4.359$).—There is a weak DLA candidate at $z = 3.04$. Si II is detected at this redshift but may be blended with C IV at $z = 3.719$.

66. *PSS J2344+0342* ($z = 4.239$).—There are two very high column density DLA candidates at $z = 2.68$ and 3.21. Both have associated metal lines.

67. *BR J2349−3712* ($z = 4.208$).—There is a weak DLA candidate at $z = 3.69$ with associated Si II.

9. CONCLUSIONS

We have presented the spectra of 66 $z \gtrsim 4$ bright quasars with ~ 5 Å resolution (FWHM) and signal-to-noise ratio ranging from 10 to 30. Twenty-six new damped Lyα absorption candidates (column densities $N_{\rm H\,I} \geq 2 \times 10^{20}$ atoms cm^{-2}) and 49 new Lyman-limit systems ($N_{\rm H\,I} \geq 1.6 \times 10^{17}$ atoms cm^{-2}), 15 of which are within 3000 km s^{-1} of the quasar emission, have been discovered. The space density and column density evolution of these systems will be analyzed in subsequent papers. Higher resolution observations are needed in order to confirm the column density measurement and to differentiate the multiple systems among the DLA candidates presented here, and in order to make detailed analysis of the metallicity content of these absorbers. These high-column density systems can also be used to measure the neutral hydrogen content of the universe over a large redshift range, thus probing the formation epoch of these objects and tracing the gas from which stars form. Analyzed in conjunction with previous studies, our new survey will provide enough data to help draw statistically more significant conclusions on these issues at high redshift.

The authors are indebted to the referee, Julia Kennefick, for helpful comments. C. P. warmly thanks Max Pettini for useful suggestions on an earlier version of this manuscript, Bob Carswell for help with his code, and PPARC and the Isaac Newton Trust for support. L. S. L. is grateful to the staff at CTIO for their expert assistance in obtaining some of the observations presented here. R. G. M. would like to thank the Royal Society for support. This research has made use of the NASA/IPAC Extragalactic Database (NED), which is operated by the Jet Propulsion Laboratory, California Institute of Technology, under contract with the National Aeronautics and Space Administration. This paper is based on observations obtained at the William Herschel Telescope which is operated on the island of La Palma by the Isaac Newton Group in the Spanish Observatorio del Roque de los Muchachos of the Instituto de Astrofisica de Canarias, on observations made at the Cerro Tololo Intra-American Observatory which is operated by the Association of Universities for Research in Astronomy, under a cooperative agreement with the National Science Foundation as part of the National Optical Astronomy Observatories and on data obtained at the W. M. Keck Observatory, which is operated as a scientific partnership among the California Institute of Technology, the University of California, and the National Aeronautics and Space Administration. The Observatory was made possible by the generous financial support of the W. M. Keck Foundation.

REFERENCES

Abel, T., & Mo, H. 1998, ApJ, 494, L151
Bergeson, S., & Lawler, J. 1993, ApJ, 414, L137
Cardelli, J. A., Meyer, D. M., Jura, M., & Savage, B. D. 1995, ApJ, 452, 275
Cole, S., Aragon-Salamanca, A., Frenk, C., Navarro, J., & Zepf, S. 1994, MNRAS, 271, 781
Dessauges-Zavadsky, M., D'Odorico, S., McMahon, R. G., Molaro, P., Ledoux, C., Peroux, C., & Storrie-Lombardi, L. J. 2000, A&A, submitted
Fan, X., et al. 1999, AJ, 118, 1
Fan, X., et al. 2000, AJ, 120, 1167
Francis, P., Hewett, P., Foltz, C., Chaffee, F., Weymann, R., & Morris, S. 1991, ApJ, 373, 465
Gunn, J. E. & Peterson, B. A. 1965, ApJ, 142, 1633
Hall, P. B., Osmer, P. S., Green, R. F., Porter, A. C., & Warren, S. J. 1996, ApJ, 462, 614
Henry, J. P., et al. 1994, AJ, 107, 4
Hook, I. M., et al. 2001, in preparation
Jimenez, R., Bowen, D. V., & Matteucci, F. 1999, ApJ, 514, L83
Kauffmann, G., & Haehnelt, M. 2000, MNRAS, 311, 576
Kauffmann, G., White, S., & Guiderdoni, B. 1993, MNRAS, 264, 201
Kennefick, J., De Carvalho, R., Djorgovski, G., Wilber, M., Dickson, E., & Weir, N. 1995a, AJ, 110, 78
Kennefick, J., Djorgovski, S., & De Carvalho, R. 1995b, AJ, 100, 2553
Lanzetta, K. M., Wolfe, A. M., Turnshek, D. A., Lu, L., McMahon, R. G., & Hazard, C. 1991, ApJS, 77, 1
Lanzetta, K. M., Wolfe, A. M., & Turnshek, D. A. 1995, ApJ, 440, 435
Ledoux, C., Petitjean, P., Bergeron, J., Wampler, E., & Srianand, R. 1998, A&A, 337, L51
Levshakov, S., Agafonova, I., & Kegel, W. 2000, A&A, 355, L1
Lu, L., Sargent, W. L. W., & Barlow, T. A. 1998, AJ, 115, 55
Matteucci, F. Molaro, P., & Vladilo, G. 1997, A&A, 321, 45
McMahon, R. G., et al. 2001, in preparation
Molaro, P., Bonifacio, P., Centurion, M., & Vladilo, G. 1999, A&A, 349, L13
Morton, D. 1991, ApJS, 77, 119
Nussbaumer, H., Pettini, M., & Storey, P. 1981, A&A, 102, 351
Peroux, C., et al. 2001, in preparation
Pettini, M., Smith, L., King, D., & Hunstead R. 1997, ApJ, 486, 665
Prochaska, J. X., & Wolfe, A. 1998, ApJ, 507, 113
———. 2000, ApJ, 533, L5
Rao, S. M., & Turnshek, D. A. 2000, ApJS, 130, 1
Sargent, W. L. W., Steidel, C. C., & Boksenberg, A. 1989, ApJS, 79, 703
Schneider, D. and the Quasar Absorption Line Key Project. 1993, ApJS, 87, 45
Somerville, R., Primack, J., & Faber, S. 2000, MNRAS, 320, 504

Songaila, A., Hu, E., Cowie, L., & McMahon, R. G. 1999, ApJ, 525, L5
Steidel, C., Dickinson, M., & Persson, S. 1994, ApJ, 437, L75
Stengler-Larrea, E. A., et al. 1995, ApJ, 444, 64
Stern, D., Djorgovski, S. G., Perley, R. A., de Carvalho, R. R., & Wall, J. V. 2000, AJ, 119, 4
Storrie-Lombardi, L. J., Irwin, M. J., & McMahon, R. G. 1996a, MNRAS, 282, 1330
Storrie-Lombardi, L. J., Irwin, M. J., McMahon, R. G., & Hook, I. M. 2001, MNRAS, in press
Storrie-Lombardi, L. J., McMahon, R. G., & Irwin, M. J. 1996b, MNRAS, 283, L79
Storrie-Lombardi, L. J., McMahon, R. G., Irwin, M. J., & Hazard, C. 1994, ApJ, 427, L13
———. 1996c, ApJ, 468, 128
Storrie-Lombardi, L. J., & Wolfe, A. M. 2000, ApJ, 543, 552
Warren, S. J., Hewett, P. C., & Osmer, P. S. 1991, ApJS, 76, 23
Wolfe, A., Turnshek, D., Smith, H., & Cohen, R. 1986, ApJS, 61, 249
Zickgraf, F.-J., Voges, W., Krautter, J., Thiering, I., Appenzeller, I., Mujica, R., & Serrano, A. 1997, A&A, 323, L21